



universität
wien

DIPLOMARBEIT

Titel der Diplomarbeit

Generation and Classification of Airborne Molecular Clusters

angestrebter akademischer Grad

Magister der Naturwissenschaften (Mag.rer.nat)

Verfasserin: Daniela Wimmer

Matrikel-Nummer: 0202684

Studienrichtung (lt. Studienblatt): Physik A411

Betreuer: Ao. Univ.-Prof. Dr. Georg Reischl

Wien, am 5. November 2008

Acknowledgements

I would like to thank

- Dr. Georg Reischl for supervising my diploma thesis and for all the interesting personal and scientific discussions
- my colleague Mag. Gerhard Steiner for his patience and his support during the whole work
- Dr. Regina Hitzemberger for her kind support and the numerous discussions during my work
- Dr. Michel Attoui for the measurements performed together and for introducing me into the use of his equipment

Above all, I want to thank my parents for supporting my studies and especially my best friends the $\phi\alpha\kappa$ (Fabienne Eder, Claudia Lederer, Silvia Pabisch, Gabriele Schätzel and Barbara Wünschek) without whom I would never have been able to finish my studies.

Abstract

Recently, the behavior of nanometer sized particles down to molecular clusters has become of special interest for numerous scientific fields (material sciences, sensor technology, atmospheric particle formation, biophysics, physical chemistry, measurement techniques of small particles, etc.). For basic studies performed under laboratory conditions, the characterization as well as the generation of well-defined nano-aerosols with sizes down to single molecules is of crucial importance. Further, the physical properties and chemical nature of the generated aerosols have to be known and/or controlled as different experimental studies require different particle properties. Therefore this work gives an overview of different cluster generation techniques with an in depth evaluation of the electrospray method.

The electrospray generator used throughout this work proved long time stability regarding generated cluster concentration as well as generated particle size distribution. As the number size distributions (NSD) of electrosprayed solutions of Tetraalkyl ammonium halide salts dissolved in high grade alcohols show several uniquely identifiable monomobile cluster species, they are well qualified for numerous applications in aerosol science. In combination with an appropriate high resolution classifier an electrospray is an excellent tool for studies where high quality monodispersed/monomobile particles are of crucial importance.

Zusammenfassung

Seit geraumer Zeit ist das Verhalten von Partikel im Nanometerbereich bis zu molekularen Clustern von besonderem Interesse für viele Wissenschaftsbereiche (Materialforschung, Sensortechnologie, Partikelbildung in der Atmosphäre, Biophysik, physikalische Chemie, Messtechnik für kleine Partikel, etc.). Für Grundlagenforschung unter Laborbedingungen ist die Charakterisierung wie auch Generierung von wohldefiniertem "Nano-Aerosol", mit Größen die bis in den Bereich von molekularen Clustern reichen, von entscheidender Bedeutung. Da verschiedene experimentelle Untersuchungen unterschiedliche Partikeleigenschaften erfordern, müssen sowohl physikalische wie chemische Eigenschaften der generierten Partikel bestimmt und kontrolliert werden. Daher soll diese Arbeit einen Überblick über verschiedene Techniken zur Clustergenerierung mit einer detaillierten Evaluierung der Electrospray Methode geben.

Der in dieser Arbeit benutzte Electrospray Generator bewies Langzeitstabilität sowohl bezüglich generierter Clusterkonzentration wie auch Partikelgrößenverteilung. Da die Korngrößenverteilung von Tetraalkylammoniumhalidsalzen, gelöst in qualitativ hochwertigen Alkoholen, erzeugt mit der Electrospray Methode, mehrere voneinander getrennt identifizierbare monomobile Clusterspezies aufweist, sind diese Substanzen hervorragend geeignet für verschiedene Anwendungen aerosolbezogener Forschung. In Kombination mit einem geeigneten hoch auflösenden Klassifikator ist ein Electrospray Generator ein ausgezeichnetes Werkzeug für Studien, die wohldefinierte monodisperse bzw. monomobile Partikel erfordern.

Contents

Acknowledgments	3
1 Motivation	11
2 Cluster Generators	13
2.1 Electrospray	13
2.1.1 Principle of Operation	13
2.1.2 De La Mora Type Electrospray Generator	15
2.1.3 Vienna Modified De la Mora Type Electrospray	16
2.2 WO _x -Generator	19
2.3 Glowing Wire Generator	20
2.4 Spark Generator	23
2.5 Ion Cluster Sources	26
2.5.1 ²⁴¹ Am Neutralizer	27
2.5.2 Corona Charger	27
3 Classification of Clusters	29
3.1 Electrostatic Mobility Spectrometry	29
3.1.1 UDMA	32
4 Experimental Setup	38
4.1 Electrospray Setup	38
4.2 Diffusion Chargers Setup	40

5	Experimental Results	42
5.1	Electrospray	42
5.1.1	Background Measurements	42
5.1.2	Tetraheptylammonium Bromide	43
5.1.3	Tetrabutylammonium Iodide	46
5.1.4	Tetrapentylammonium Iodide	48
5.1.5	Tetradodecylammonium Bromide	51
5.1.6	Nucleation Experiments	53
5.2	Ion Cluster Sources	58
5.2.1	Diffusion Charger Ions	58
5.2.2	Electrosprayed Water Clusters	59
6	Discussion	61
6.1	Feasibility of the Electrospray	61
6.2	Kilpatrick's mass-mobility Relationship	62
6.3	Corona Discharge from Electrospray	64

Chapter 1

Motivation

Recently, the behavior of nanometer sized particles down to molecular clusters has become of special interest for numerous scientific fields (material sciences, sensor technology, atmospheric particle formation, biophysics, physical chemistry, measurement techniques of small particles, etc.). For basic studies performed under laboratory conditions, the characterization as well as the generation of well-defined nano-aerosols with sizes down to single molecules is of crucial importance. Further, the physical properties and chemical nature of the generated aerosols have to be known and/or controlled as different experimental studies require different particle properties. Therefore well controllable generation techniques for molecular clusters are required.

The most suitable method to determine the number size distribution (NSD) of ultrafine particles is the Electrostatic Mobility Spectrometry (EMS). The EMS classifies particles according to their electrical mobility. The Differential Mobility Analyzer (DMA) is the most important component of an EMS. In combination with an appropriate aerosol generator, the DMA can also be used as a source of well-defined monodisperse particles.

In the last few years high flow, high resolution DMAs optimized to measure the mobility distribution of molecular clusters have been developed. In principle a DMA is designed in form of a capacitor (mainly cylindrical) and is specified by two groups of parameters. At fixed geometry parameters and operating conditions (flow conditions),

a unique correlation exists between the adjusted electrode voltage and the electrical mobility of the classified particles. However high resolution DMAs are typically characterized by a relatively short channel length and large flow rates; both difficult to be determined. To provide the correlation between mobility and applied voltage at unknown but fixed flow rates a further calibration with mobility primary standards generated by an adequate particle source is required.

For laboratory studies on heterogeneous nucleation of atmospheric relevant vapors on aerosol seed particles, the generation of extremely monodispersed particles is of crucial importance. The classical method is to extract a narrow mobility fraction from a broad NSD, produced by an appropriate aerosol generator. To extend this method into the size range of molecular clusters it is necessary to apply a particle source already providing monomobile clusters.

This work should give an overview of the most widely used nano-particle generation methods, required for the above mentioned experimental needs. Stability, possible size ranges and achievable number concentrations will be discussed. Advantages and disadvantages of various generators will be pointed out.

Chapter 2

Cluster Generators

2.1 Electrospray

2.1.1 Principle of Operation

The electrospray method is widely used for the generation of well-defined nanometer sized particles down to single molecules.

In principle an electrospray generator consists of a capillary housed in an electrospray chamber. A liquid sample is pushed through the capillary by a pressure support. The liquid sample is raised to a high voltage potential while the electrospray chamber is grounded. As the liquid reaches the tip of the capillary, the electric field induces a surface charge on the liquid. The electrostatic charge of the liquid produces forces that cause the liquid to disperse into a fine spray of charged droplets (figure 2.2). To reduce the number of elementary charges on the particles some designs contain a neutralizing device within the electrospray chamber. The liquid flow rate $\dot{V}[\frac{m^3}{s}]$ through the capillary is governed by the equation for a Poiseuille flow in a circular tube:

$$\dot{V} = \frac{\pi \cdot r^4}{8 \cdot \eta} \cdot \frac{\partial p}{\partial z}$$

where:

r ... inner radius of the capillary [m]

η ... dynamic viscosity of the liquid [Pas]

z ... flow direction

After the formation of the highly charged primary droplets the solvent liquid evaporates resulting in a coulomb explosion when the Rayleigh charge limit is exceeded [1, 2, 3].

Two parameters limit the size and the charge of the remaining particles; Rayleigh's charging limit q_R for a drop having the surface tension σ of the solvent liquid and the radius R_i of the embedded ion.

$$e \cdot z_R = q_R(R_i) = 8 \cdot \pi \cdot \sqrt{\sigma \cdot \epsilon_0 \cdot R_i^3}$$

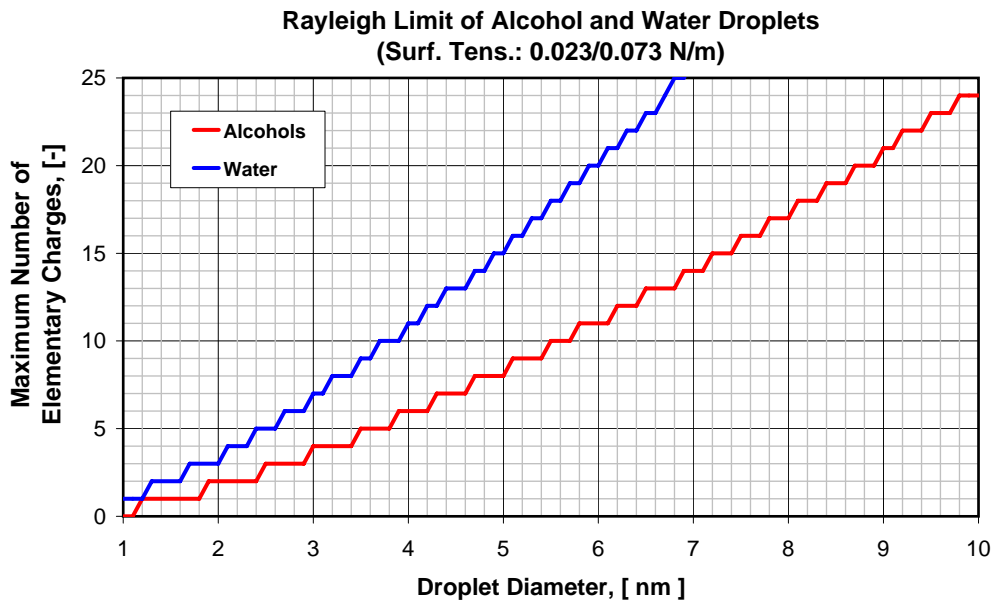


Figure 2.1: Rayleigh Limit in Dependence of Diameter for Water (blue line) and Alcohols (red line)

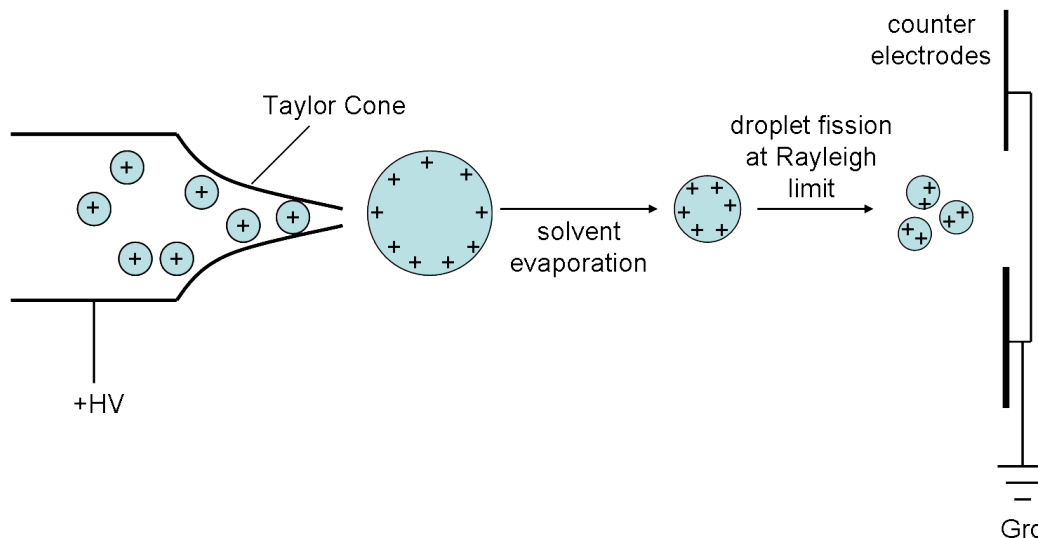


Figure 2.2: Schematic of the Ion Formation Process

2.1.2 De La Mora Type Electrospray Generator

The results presented in this work have been obtained using two different types of electrospray sources. The first was designed by Juan Fernández de La Mora [4]. The cylindrical electrospray chamber is equipped with viewing ports at both ends. An inlet and a 1/4" outlet joint are situated in the axis perpendicular to the cylinder. In the latter a silica capillary with 360 μm outer and 39 μm inner diameter is used. One end of the capillary is immersed into a vial containing the liquid sample. The capillary is housed in a bent aluminum tubing connecting the vial to the stainless steel electrospray chamber. Further the vial is connected to a pressure support in order to push the liquid sample through the needle. To connect the high voltage supply to the liquid sample, a platinum wire is immersed into the suspension. An additional gas inlet situated next to the conically shaped tip of the capillary provides the dilution gas flow. For the experiments performed in this work a dilution gas flow of dried and purified pressurized laboratory air was used. The tip of the capillary is adjusted in the center of the chamber. For the observation of the Taylor cone, it is necessary to install an external light source in front of one of the glass windows and a microscope with a suitably long working distance on the opposite window. Compared to commercial

designs the advantage of this type of electrospray source is the compact size and the simple way to adjust the operating parameters. Further it proved to feature long time stability of output cluster concentrations.

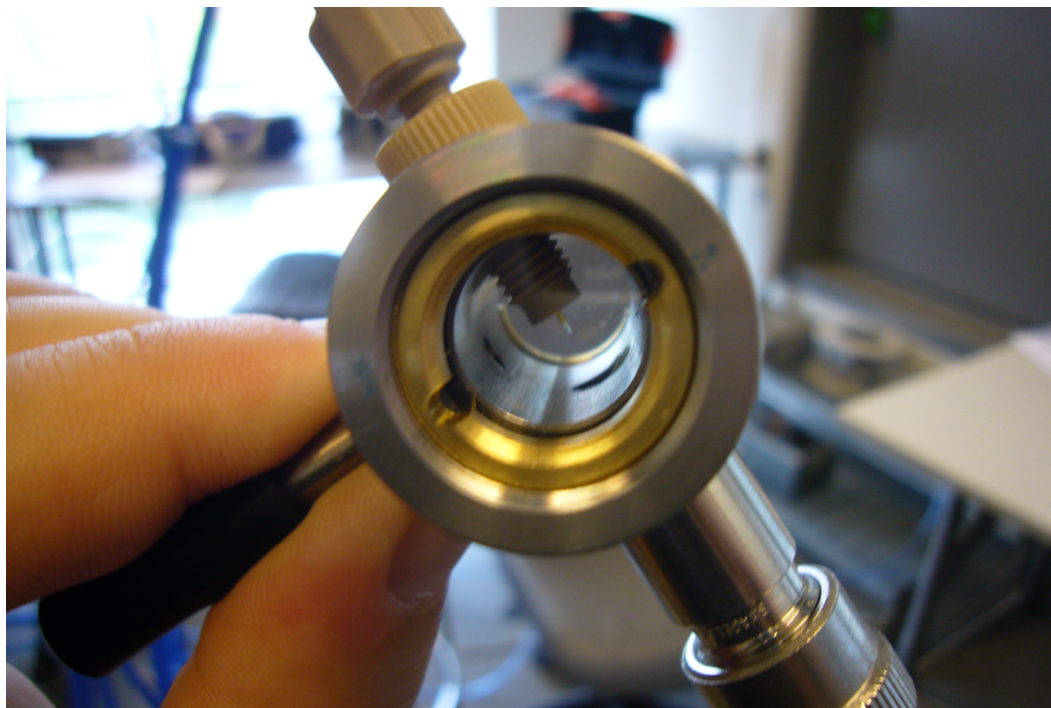


Figure 2.3: Viewing Part of the Fernández de la Mora Electrospray

2.1.3 Vienna Modified De la Mora Type Electrospray

The Vienna type electrospray generator is a slightly modified version of the design presented by Juan Fernández de la Mora [4]. The main idea for a redesign was to improve the observation technique of the interior of the electrospray chamber. For this purpose an LED light source and an optical system with a high resolution microscope camera ($3 \cdot 10^6$ pixel) are implemented to the generator. Furthermore all metallic parts are manufactured of stainless steel to avoid any chemical reactions. A silica capillary of $39 \mu m$ in inner diameter and a length of 20 cm is shaped to a conical tip on one end. It is housed in a 6 mm tubing connected on one side to the grounded electrospray chamber. On the other side it ends in a T-piece connector attached to the liquid sample reservoir and a pressure support. To push the liquid sample through the capillary a pressure

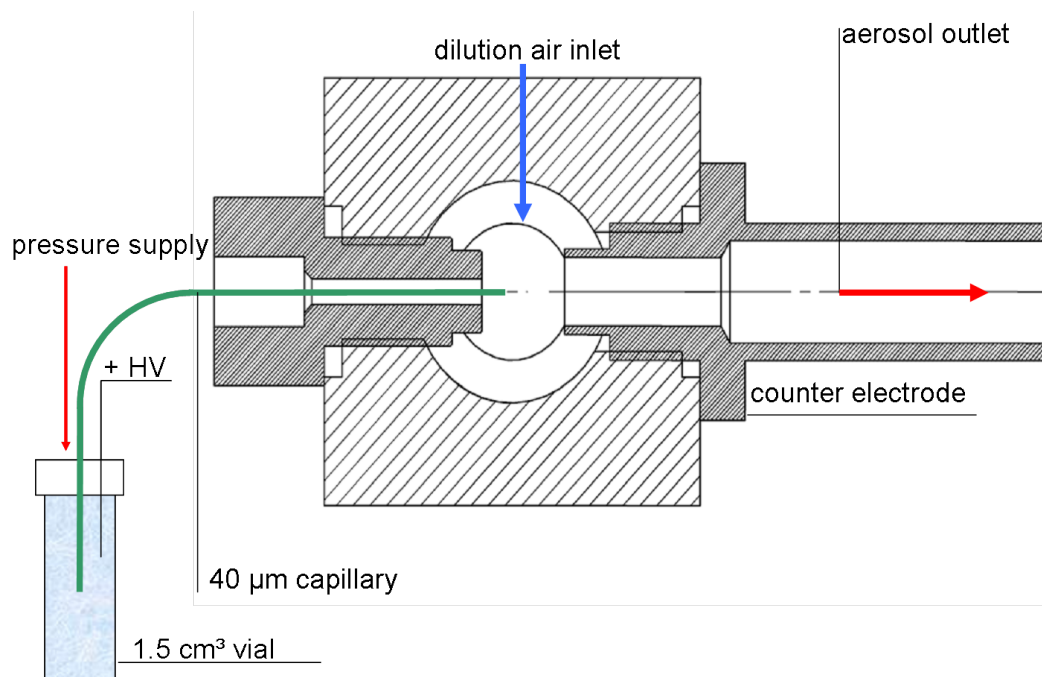


Figure 2.4: Schematic of an Electro spray

regulator with an accuracy of 100 *mbar* is used. Typically, commercially available top threaded 1.5 *cm*³ conical vials are used as containment for the liquid sample. In order to easily change the suspension a corresponding threaded cap is mounted at the T-piece. To supply the suspended sample with a high voltage potential a platinum wire is immersed into the liquid. An adjustable computer controlled high voltage power supply provides up to +5 *kV*. The outlet port connector screwed into the main body serves as counter electrode to obtain a homogeneous local electrical field inside the electro spray chamber. See figure 2.4.

Typically a pressure of 100 *mbar* is adjusted to provide the liquid flow rate through the capillary. On the top of the electro spray chamber, two dilution air inlets are located in the vicinity of the tip of the needle. As they are positioned eccentrically to the capillary's axis, an additional aerodynamic focusing of the dilution air flow to the generator outlet port is obtained. Usually a dilution air flow of 17 sl/min of purified and dried pressurized laboratory air is used. As already mentioned, the improved optical system consists of an inbuilt LED light source with a diffuser plate and a convex lens with a focal length of 20 mm. A length variable tube of approximately 20 cm is mounted

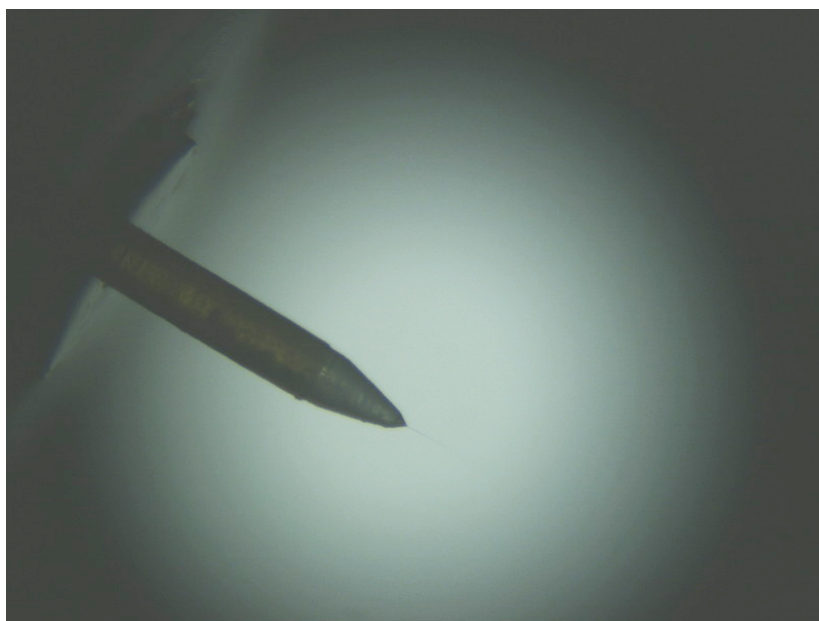


Figure 2.5: Closeup of the interior of the Electrospray chamber. It shows the conical tip of the capillary and the liquid jet emanating from the triangular shaped Taylor cone.

between the magnification lens and the microscope camera to adjust the focal point.

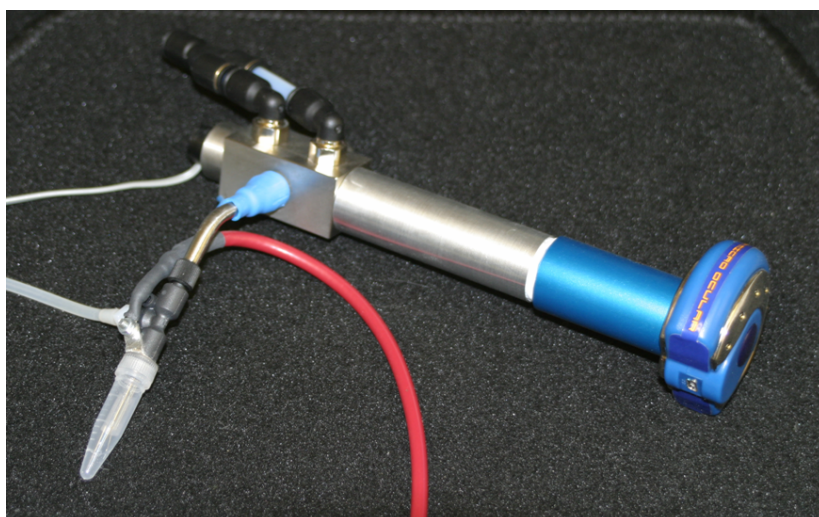


Figure 2.6: Picture of the slightly modified Electrospray Generator

2.2 WO_x -Generator

Another Cluster Generator producing particles in the size range below 5 nm, is a heating wire particle generator based on the sublimation of tungsten oxide, the so called WO_x Generator. Picking up the idea of a prototype WO_x -Generator built at the Institute of Chemical Kinetics and Combustion in Novosibirsk [5, 6], an improved version was developed at the University of Vienna [7] in cooperation with Grimm-Aerosoltechnik GmbH & Co. KG and finally made commercially available as 7.860 tungsten oxide generator. Heated tungsten reacts in dry clean air to several oxides and nitrates. A heating cell around the WO_x coil provides a temperature of approximately 900°C; the sublimation temperature of WO_3 , appearing as a bright yellowish substance. Tungsten oxide sublimates into a controlled fraction of the carrier gas and is immediately diluted when exiting the heated zone by a flow of purified air. By means of three adjustable flows (WO_x air, carrier air and diluting air) and a variable heating source, the mean diameter and output concentration of the aerosol can be controlled in

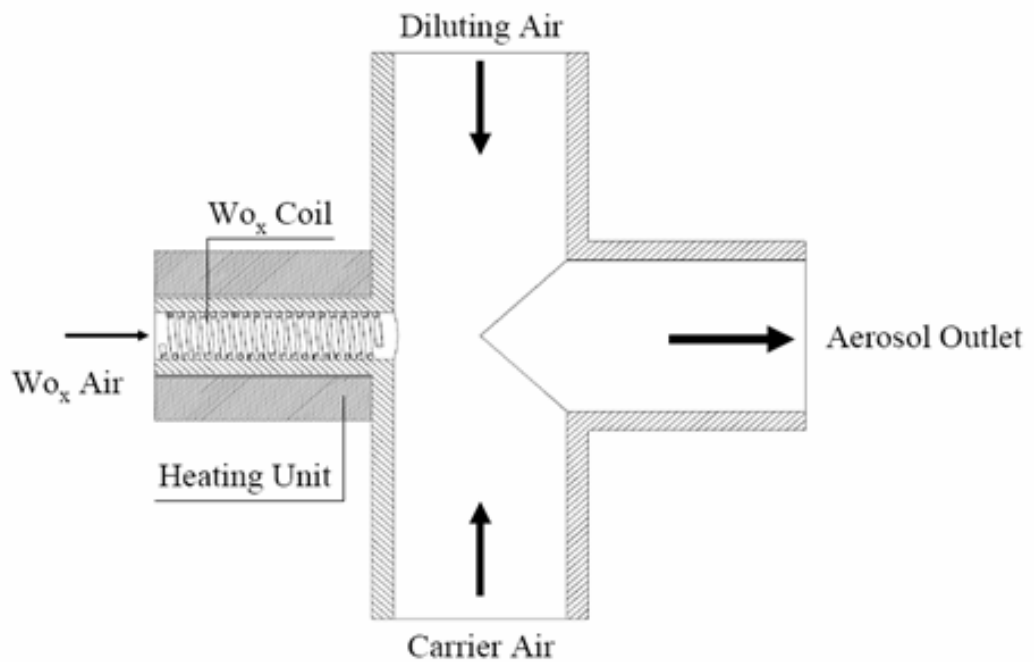


Figure 2.7: Schematic of the WO_x Generator's Heating Zone

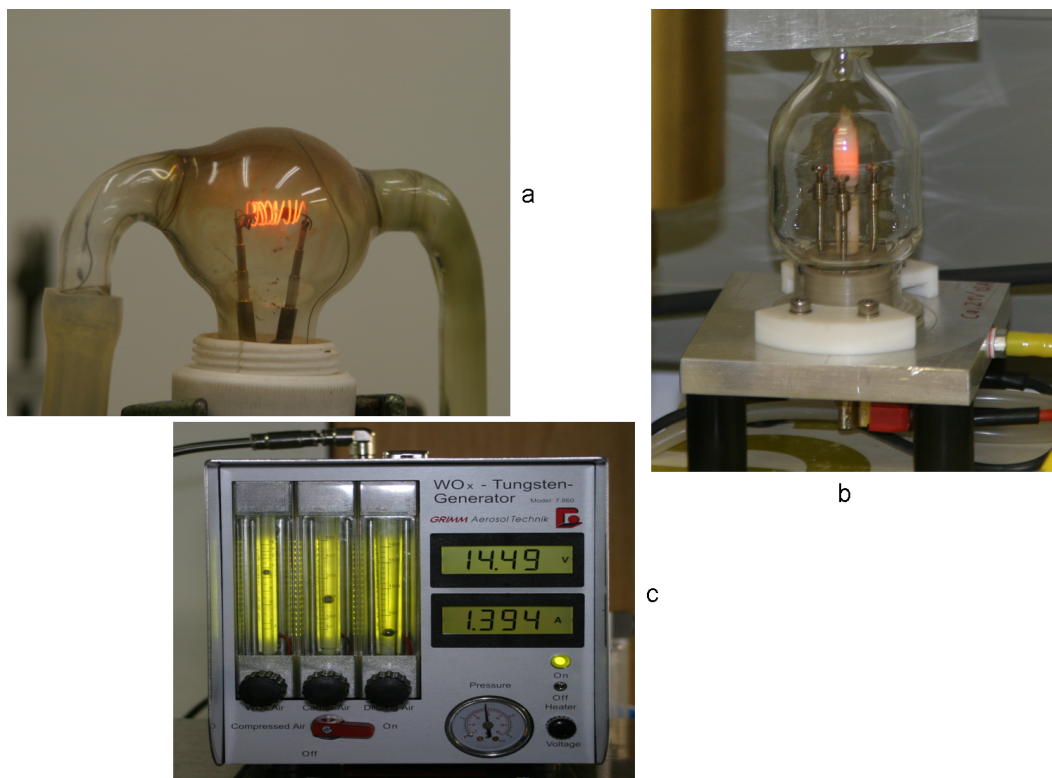


Figure 2.8: Evolution of the WO_x Generator, a shows the Novosibirsk type built at the Institute of Combustion, b shows the Vienna prototype, built at the University of Vienna and c shows the commercially available 7.680 tungsten oxide generator

a size range from 1.2 nm to 10 nm [8]. Due to its high atomic weight, single molecules of tungsten oxide have a mobility equivalent diameter of 1.25 nm. Consequently, this substance is highly qualified as cluster source in this size range.

2.3 Glowing Wire Generator

In the glowing wire generator (GWG), material is sublimated by passing a high current through a conducting wire. Nano-particles are produced by homogeneous nucleation of the sublimated supersaturated vapor. The vapor is rapidly diluted by a purified gas flow to avoid clustering and coagulation. The GWG presented by Peineke et al. [9] is mainly built of standard stainless steel UHV (ultra high vacuum) parts. Figure 2.9 shows a schematic of the instrument. The wire is mounted in a four way cross

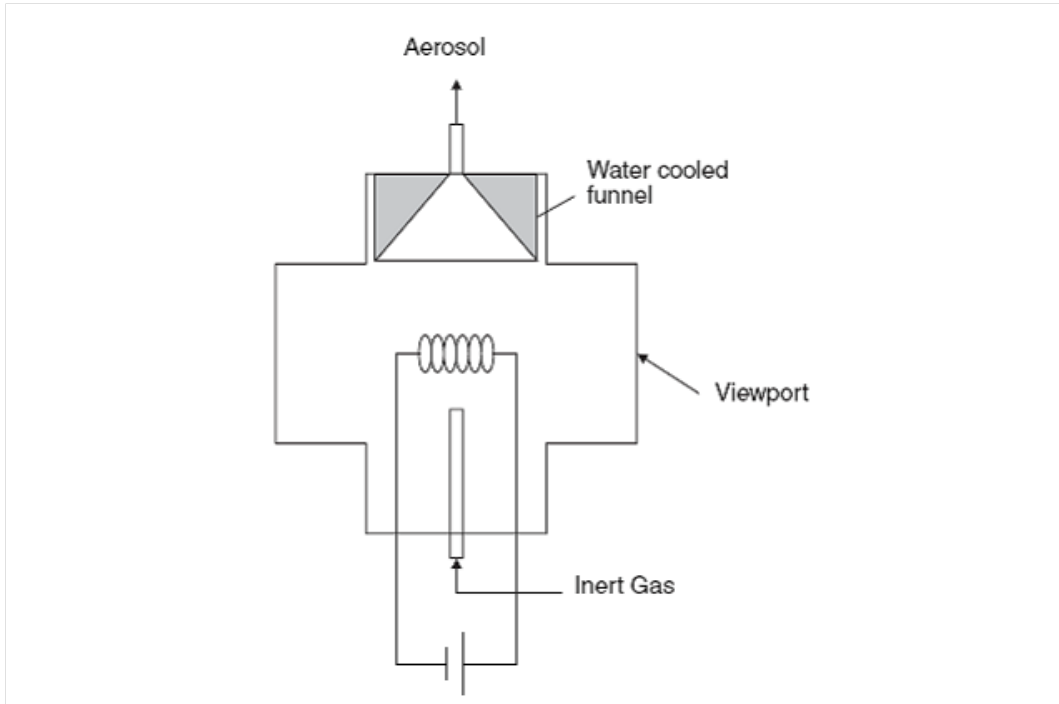


Figure 2.9: Schematic of the Glowing Wire Generator [9]

between two current feedthroughs. Two flanges are equipped with a gas inlet and aerosol outlet, respectively. The remaining flange is equipped with a view port. The wire is resistively heated close to its melting temperature by a DC low voltage/high current supply according to Ohm's law:

$$P_{wire} = \frac{U_{wire}^2}{R_{wire}}$$

In the literature successfully working GWG setups are reported for Ag, Fe, Be, Ni, Pt, Pd, W, Nb, Co and Zr. The range of possible particle diameters and concentrations can be controlled by the dilution air flow and the heating power. Typical achievable mean diameters are in the size range between 1-10 nm. Furthermore, a large fraction of charged particles is produced due to the formation process.

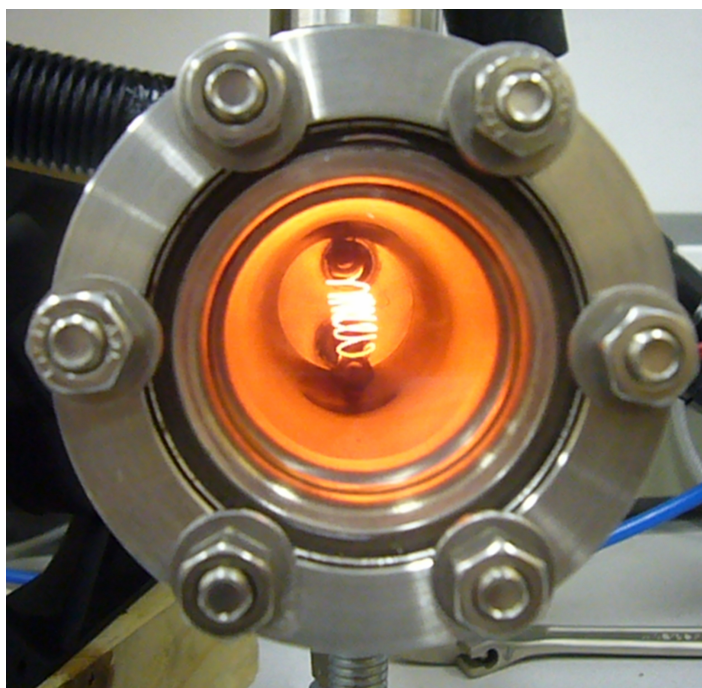


Figure 2.10: Glowing Wire Generator Working

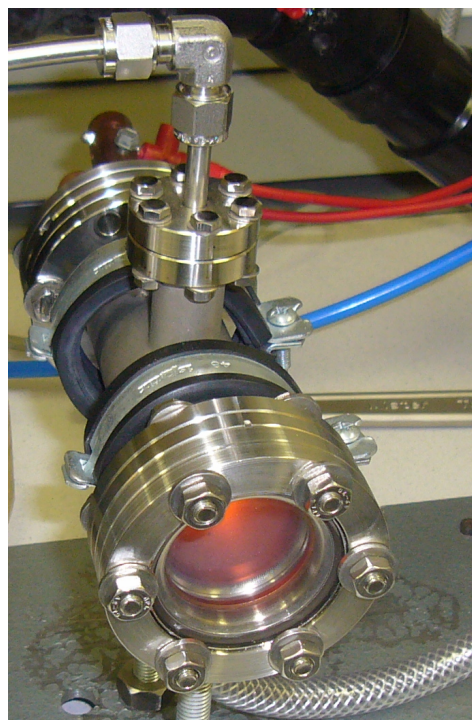


Figure 2.11: Picture of the Glowing Wire Generator

2.4 Spark Generator

Schwyn et al., [10] introduced the method of generating metallic particles by a spark discharge between two electrodes of the respective material. The highly localized spark energy causes the electrode material to evaporate resulting in the subsequent formation of particles by homogeneous and heterogeneous nucleation processes [10]. A similar method is used to produce carbonaceous particles.

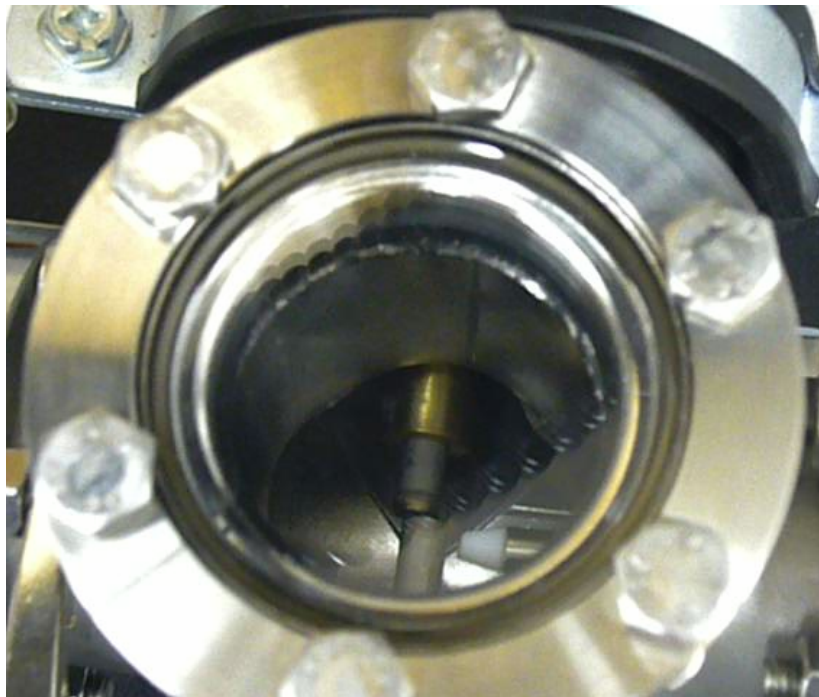


Figure 2.12: Insight of the Spark Generator

Similar to the glowing wire generator described above, the SPG (spark generator) designed by Schmidt-Ott [11] mainly consists of standard stainless steel UHV parts to avoid contamination by surface impurities. The electrodes are mounted in a five way cross where two flanges serve as gas inlet and aerosol outlet. In the perpendicular axis two flanges contain the adjustable high voltage feedthroughs for the electrodes. The remaining flange of the SS cross is equipped with a view port. Typically, cylindrical Al, Cu and graphite electrodes with a diameter of 6 mm are used. A high voltage capacitor is continuously charged by a high voltage power supply operated in a constant current mode (12 kV-10 mA maximum). Once the breakthrough voltage (several thousands to

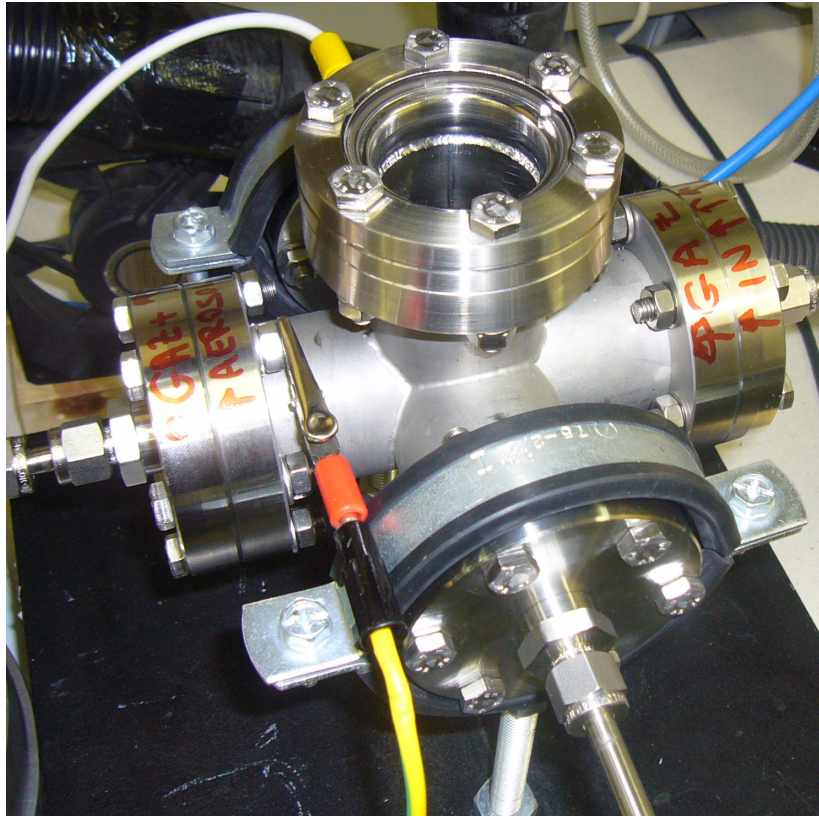


Figure 2.13: Spark Generator

ten thousands Volts) between the electrodes is reached, the capacitor is discharged by the spark.

For a stable operation of the generator the distance between the electrodes, their shape and the gas in between are of crucial importance since these parameters determine the breakthrough voltage. Furthermore the energy stored in the capacitor and the frequency of the sparks are determined by the electrodes distance, too. Therefore, in more sophisticated designs, the distance between the electrodes is regulated by a feedback mechanism [12, 13]. In any case the frequency of the discharges can be adjusted by the charging current. Non-reactive gases like Helium or Argon are required to produce pure carbonaceous or metallic particles. Further investigations by Attoui [14] were carried out with a high flow high resolution DMA designed for ions and nano-particles [15].

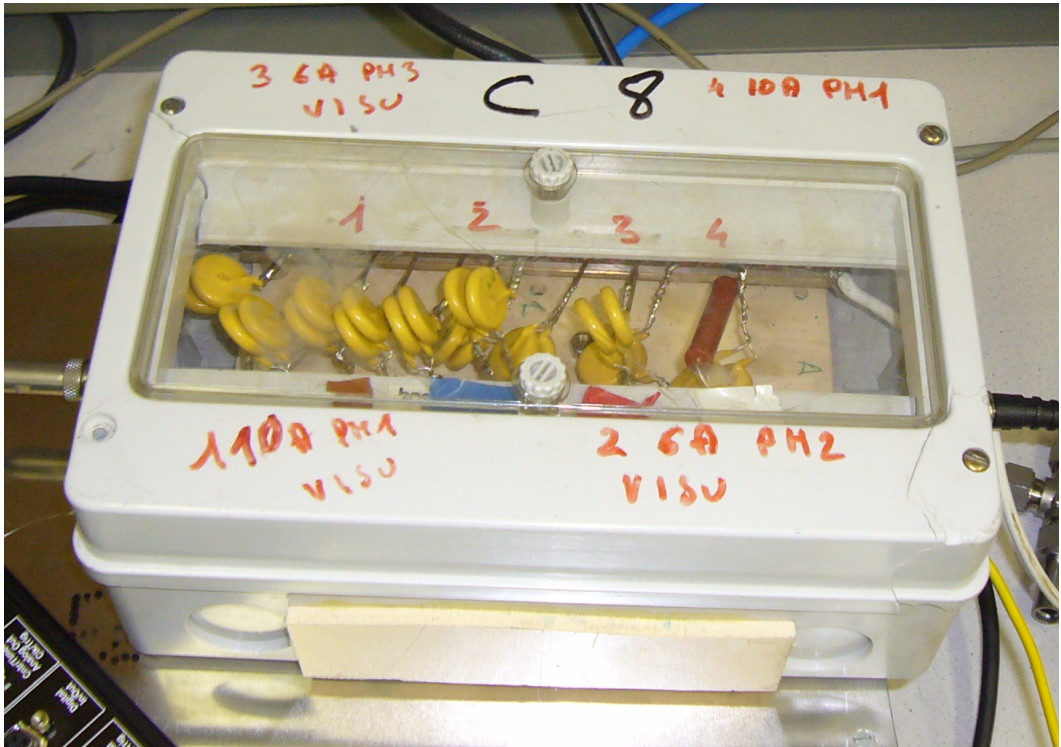


Figure 2.14: Control Device for the Spark Generator



Figure 2.15: High Voltage Supply for the SPG

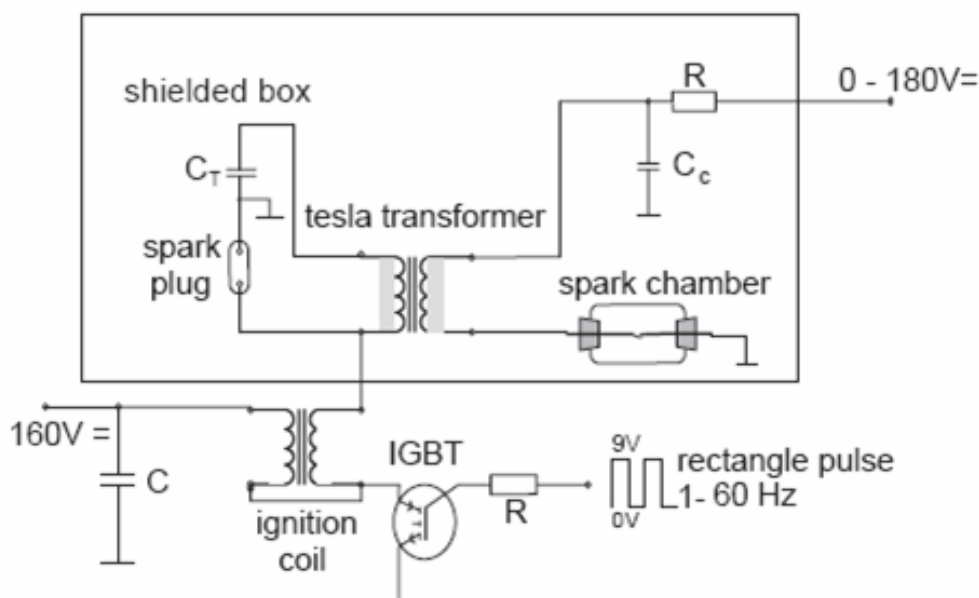


Figure 2.16: Schematic of the Spark Generator [13]

2.5 Ion Cluster Sources

The electrostatic mobility spectrometry depends on a well-defined charging state of the analyzed particles/clusters. The most widely used methods to charge and/or neutralize aerosol particles are bipolar diffusion charging by radioactive sources and unipolar diffusion charging by corona discharge. In both methods gas molecules are first ionized by an ionizing radiation forming primary ions which subsequently combine with polar molecules present in the carrier gas to build larger ionic clusters. These clusters finally combine with the aerosol particles resulting in a stationary charging state which can be calculated by well established theoretical models (e.g. Fuchs' theory) [6, 16]. All theoretical models depend on the exact knowledge of the physical properties of the charging molecular ionic clusters namely ion mobilities and ion masses which have to be determined experimentally. A superior feature of bipolar charging is the independence of particle material.

2.5.1 ^{241}Am Neutralizer

The cylindrical design of the neutralizer contains a one side ^{241}Am coated Ag stripe mounted on the inside wall of the housing, with an activity of 46.25 MBq . ^{241}Am predominately decays by emitting alpha radiation to ^{237}Np . However a small amount of gamma radiation is emitted, too.

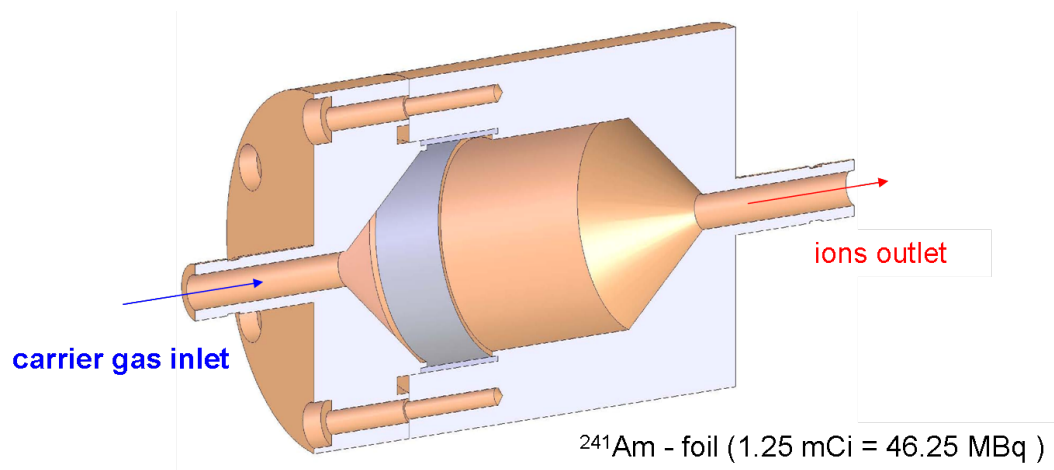


Figure 2.17: Sketch of a Bipolar Am-241 Charger

2.5.2 Corona Charger

In the corona charging method the primary ions are produced by corona discharge. Electrons or positively charged ions are emitted from the tip of a metal needle raised to a high voltage potential with respect to the grounded housing. The primary ions are a mixture of ionized gas molecules and corona ions. Similar to the processes occurring in a bipolar charging containing a radioactive source, larger ionic clusters are formed by the combination of the primary ions with polar carrier gas molecules. In this work a very simple design of a unipolar corona generator was used where a stainless steel needle is mounted in one flange of a grounded three way copper t-piece. The two other flanges are used as inlet and outlet ports for the gas flow passing through. To obtain variable ion cluster concentrations, computer controlled high voltage power supplies with maximum voltages of $\pm 10\text{ kV}$ have been used. More sophisticated designs

presented in the literature feature also bipolar diffusion charging. This method bears the great advantage of neutralizing aerosol particles without the use of radioactive sources. However, with this method the high charging efficiencies of radioactive sources based neutralizers have not been reached so far.

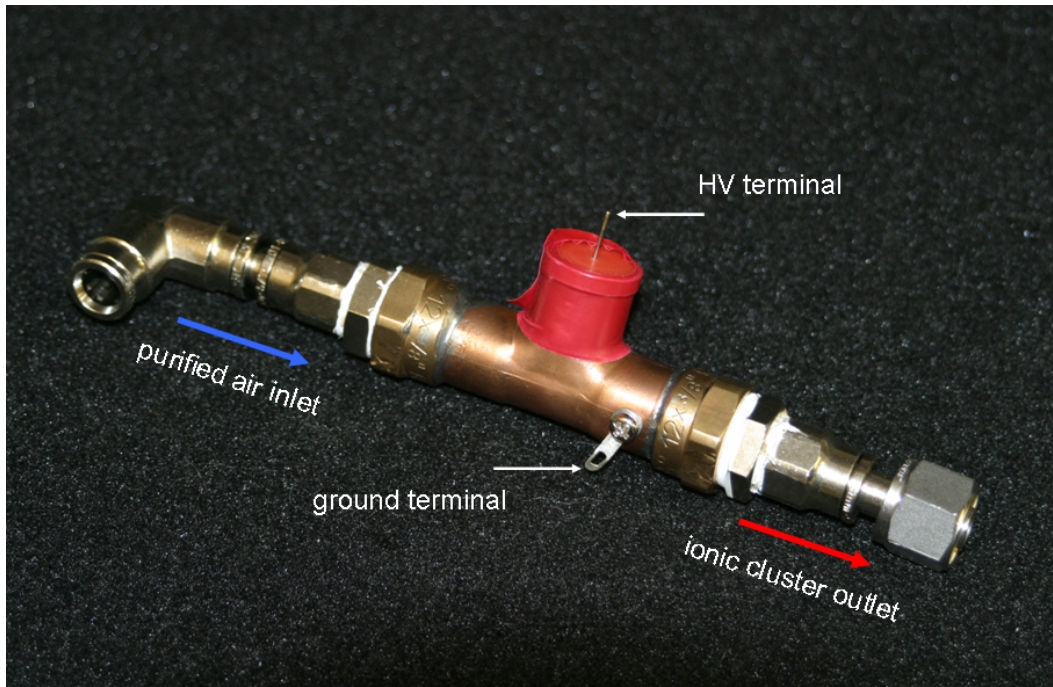


Figure 2.18: Unipolar Corona Charger

Chapter 3

Classification of Clusters

3.1 Electrostatic Mobility Spectrometry

The electrostatic mobility spectrometry concentrates on the evaluation of number size distributions of charged airborne particles. The big advantage of this method is on the one hand the applicability over several orders of magnitude regarding both particle size and concentration at the same relative resolution and on the other hand the lack of influences on the aerosol by the measuring procedure. The Differential Mobility Analyzer (DMA) is the most important component of an EMS. The idea of the classification of airborne particles according to their electrical mobility goes back to Rohmann [17]. Knutson and Whitby [18, 19] improved the theory as well as the experimental methods. Nowadays at least four modern types of DMAs exist, which are called "TSI type" [18] based on the design of Hewitt [20], "Vienna type" [21, 22] as well as "French radial type" [23, 24] and "American radial type" [25, 26]. Usually, a DMA is built in form of a cylindrical capacitor. Two groups of parameters characterize the DMA:

Geometry parameters (R_2 , R_1 , L)

R_2 ... Inner radius of the outer electrode

R_1 ... Outer radius of the inner electrode

L ... Effective axial gap between aerosol inlet and aerosol outlet

Operating conditions: air flow rates (Q_{sh} , Q_a , Q_s , Q_{ex})

Q_{sh} ... Sheath air flow rate

Q_a ... Aerosol flow rate

Q_s ... Sample air flow rate

Q_{ex} ... Excess air flow rate

The only variable parameter is the adjusted voltage on the center-electrode. For the typical design, the sample aerosol will be introduced laminarily to the sheath air near the outer electrode of the DMA. The particles drift according to their electrical mobility in the direction of the electrical field (radially) as well as axially through the sheath air flow toward an annular exit slit in the center electrode. At fixed geometry parameters (R_2 , R_1 , L) and operating conditions (Q_{sh} , Q_a , Q_s , Q_{ex}), a unique correlation exists between the adjusted voltage on the center electrode and the electrical mobility of the particles which enter the slit with the sample air flow Q_s from the aerosol air flow Q_a . Mathematically, the electrical mobility is defined as:

$$Z = i \cdot e_0 \cdot B$$

with

i ... number of elementary charges

e_0 ... elementary charge, $1.602 \cdot 10^{-19}$ [As]

B ... mechanical mobility

with

$$B = \frac{C(D_p)}{3\pi \cdot \eta \cdot D_p}$$

D_p ... particle diameter

$C(D_p)$... Cunningham slip correction factor

η ... viscosity of the trace gas

$$C(D_p) = 1.0 + 2.492 \cdot \frac{\lambda}{D_p} + 0.84 \cdot \frac{\lambda}{D_p} + \exp\left(-0.43 \cdot \frac{D_p}{\lambda}\right)$$

where λ is the mean free path of the trace gas molecules

resulting in:

$$Z = \frac{i \cdot e_0 \cdot C(D_p)}{3 \cdot \pi \cdot \eta \cdot D_p} [m^2/Vs]$$

with e_0 in [As], η in [kg/m²s] und D_p in [m]

By solving the integral for the equation of the path of the particles through the cylindrical canal of the DMA and the electric field, and using air flow coordinates, the electrical mobility, can be expressed by:

$$Z = \frac{1}{V} \cdot \frac{\ln(R_2/R_1)}{2\pi L} \cdot \frac{(Q_{sh} + Q_{ex})}{2}$$

For the ideal case of symmetric operating conditions ($Q_a = Q_s$, $Q_{sh} = Q_{ex}$), the transfer function $\text{Tr}(Z)$ has the form of a isosceles triangle. Therefore, the relative full width at half maximum (ΔZ) has a minimum and the resolution of the DMA is at its maximum.

The electrical mobility can therefore be described by:

$$Z = \frac{(Q_{sh} + q_{ex})}{2} \cdot \frac{\ln(R_2/R_1)}{2 \cdot \pi \cdot L} \cdot \frac{1}{V} = Q_{sh} \cdot \frac{\ln(R_2/R_1)}{2 \cdot \pi \cdot L} \cdot \frac{1}{V}$$

Equating both expressions for the electrical mobility Z

$$\frac{i \cdot e_0}{3 \cdot \pi \cdot \eta} \cdot \frac{C(D_{p,i})}{D_{p,i}} = Q_{sh} \cdot \frac{\ln(R_2/R_1)}{2 \cdot \pi \cdot L} \cdot \frac{1}{V}$$

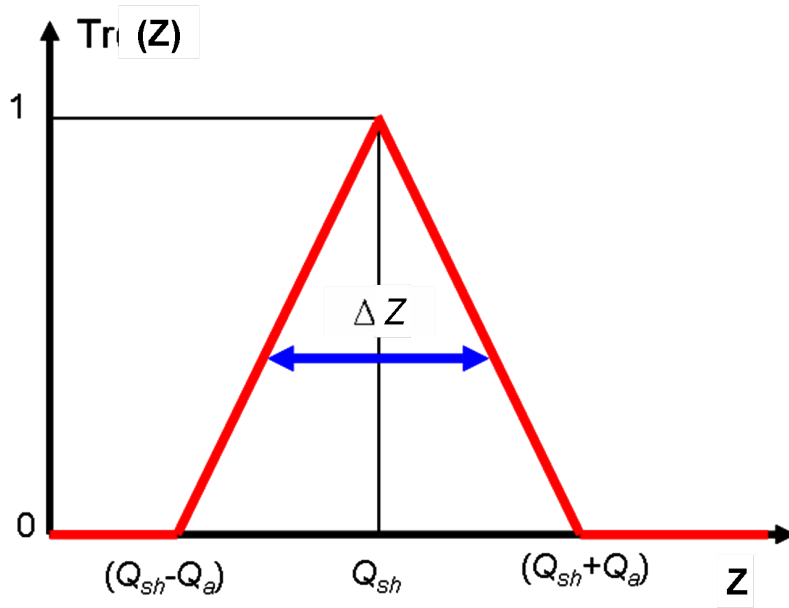


Figure 3.1: Transfer Function of the DMA $\text{Tr}(Z)$ in case of: $Q_a = Q_s, Q_{sh} = Q_{ex}$

results in the basic relation between the particle diameter and the adjusted voltage on the center electrode. In case of an extremely monodisperse aerosol, the number size distribution may be narrower than the transfer function of the DMA. Therefore, a detailed knowledge of the transfer function is necessary. As already mentioned the transfer function of the DMA has the form of an isosceles triangle at fixed symmetric operating conditions ($Q_{sh} = Q_{ex}, Q_a = Q_s$) in flux coordinates. Distortions of the transfer function, especially caused by diffusion processes of very small particles, can be calculated with numerical methods [6, 27]. In principle distortions are dependent on the geometry of the DMA as well as on the operating conditions, such as volume flow rates, carrier gas viscosity, pressure and carrier gas temperature.

3.1.1 UDMA

In the last years several authors have reported DMA designs optimized for high resolution measurements in the size range below 10 nm [28, 29, 22, 30, 31, 32]. In all designs the most important aspects are to minimize transfer function diffusion broadening and diffusion losses. Typically these DMAs are operated at increased sheath air flow rates

of several m^3/min and show a short channel length to minimize the residence time of particles in the DMA. However, they can not be easily adapted to suit the purpose of generating monodispersed clusters in a controlled clean carrier gas, since they are mostly operated as open systems. On the other hand, standard DMAs operating in a closed loop arrangement do not provide the required resolution in this size range. For the purpose of satisfying some of the above mentioned experimental needs, the typical cylindrical DMA design was improved to obtain the desired resolution without giving up the option to operate the DMA in a closed loop arrangement. The prototype of this development (UDMA, GPR-Aerosol Inc. Nevada) was used exclusively during this work (see figure 3.4). To provide the UDMA with a clean and purified sheath air flow rate up to 300 sl/min, a flow control unit consisting of four high performance membrane pumps (HYCO type ABF71/4C-7R) four silica gel diffusion dryers, four active carbon and four absolute filters was used (figure 3.6). For experiments with an increased sheath air flow rate of approximately 700 sl/min a combination of the initially described flow control with a heavy duty eight head membrane pump (HYCO type ML-130.85-ZV-D14/1.3 kW) was used (figure 3.7). Due to the relatively high sheath

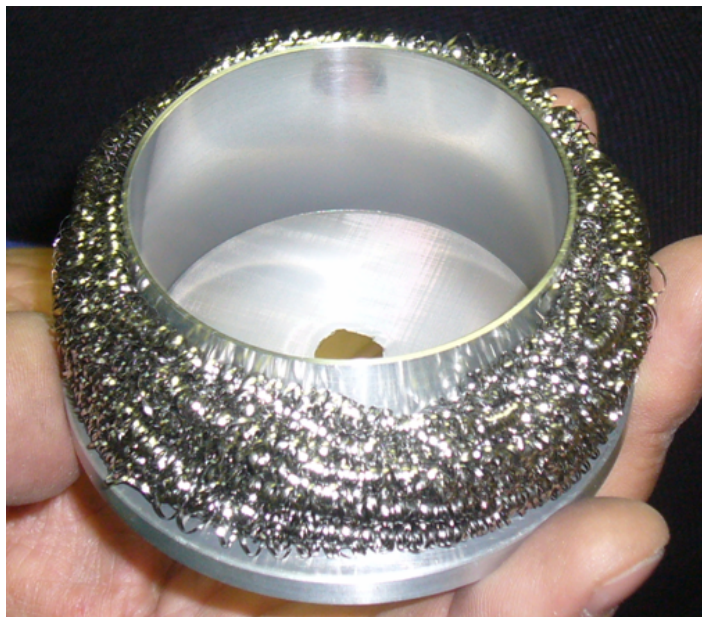


Figure 3.2: Laminarization Sponge

air flow rate, the purified sheath air Q_{sh} is introduced by four tangential stainless steel connection tubes on the top of the DMA. The interior upper part mainly consists of a cup like bracket for a 0.2 mm nylon laminarization screen. The cavity between the sheath air inlet ports and the outer side of the cup like bracket is filled with a stainless steel laminarization sponge (figure 3.2) to eliminate the tangential component of Q_{sh} to provide a uniform laminar flow through the DMA. The upper part of the channel between the electrodes is converging down to the point where the aerosol is overlaid to further accelerate the sheath air flow.

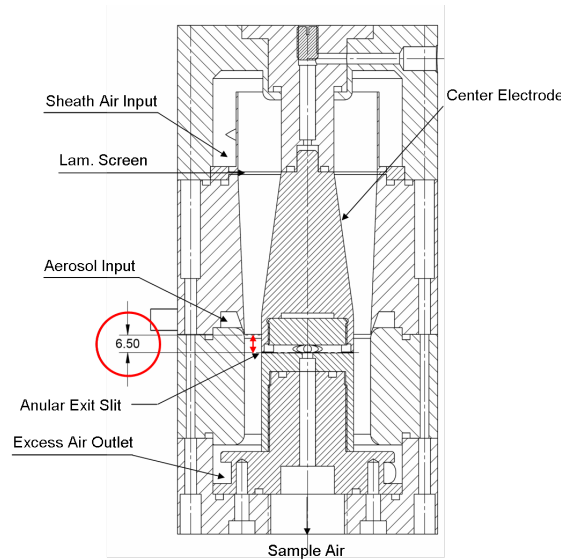


Figure 3.3: Sketch of the UDMA 2006

The aerosol inlet volume flow Q_a is fed tangentially through an inlet port in the outer electrode. A blade like shape of the inner walls and a curvature at the inner side of the outer electrode provide a smooth transition of the aerosol flow into the sheath air flow. Thus, both airflows can be merged very smoothly which is a main criterion for the classification characteristics. The classified clusters exit the DMA by a narrow annular exit slit in the center electrode and subsequently enter a directly flanged Faraday Cup Electrometer (FCE) for detection. At the bottom of the DMA, the residual air flow Q_{ex} exits the DMA by four tangential connection tubes mounted antipodal to the sheath air inlet ports. To provide the electrical field between the DMA's electrodes, a high

voltage potential (max. 10 kV) is applied to the center electrode.



Figure 3.4: UDMA 2006 and Faraday Cup Electrometer

The aerosol flow rate Q_a and the sample air flow Q_s are maintained by drawing an air flow of typically 6.5 sl/min, fixed by a critical orifice, through the FCE. Thereby an equal size inlet aerosol volume flow is provided, as the UDMA is operated under symmetric flow conditions ($Q_{sh} = Q_{ex}$ and therefore $Q_s = Q_a$). Well-defined and known operating conditions are a crucial precondition for high resolution mobility measurements. The precise determination of volumetric flow rates up to several m^3/min is very difficult and time demanding. Small deviations of the effective channel length from the nominal value have a large impact on the DMA's classification characteristics. As it is difficult to determine actual/effective channel length and actual sheath air flow rate, high flow, high resolution DMAs have to be calibrated with an adequate mobility standard. Assuming a constant but unknown sheath air flow rate Q_{sh} and channel length L , the DMA equation can be transformed to

$$Z = K \cdot \frac{1}{V}$$

where

$$K = Q_{sh} \cdot \frac{\ln\left(\frac{R_2}{R_1}\right)}{2 \cdot \pi \cdot L}$$

is the DMA's operational characterization factor. The latter can be determined experimentally by feeding aerosol particles with a well known electrical mobility to the DMA and recording the voltage where most of the particles are transferred from Q_a to Q_s (the voltage at the peak signal of the mobility spectrum). Applying this method the calibrated DMA can be operated without knowing exactly the geometric parameters and the sheath air flow rate. Primary electrical mobility standards have been presented by Ude & de La Mora using Tetraalkyl ammonium halide clusters produced by an electrospray source [33]. The latter will be discussed in detail in chapter 5.1.2. Further these monomobile clusters are highly qualified for the investigation of the performance and therefore the transfer function of a DMA (see chapter 5.1.2).

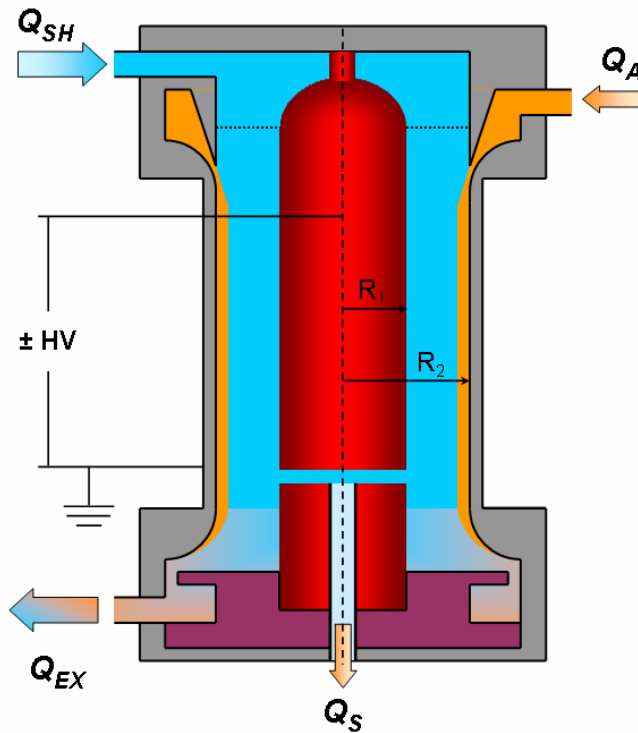


Figure 3.5: Schematic of a Cylindrical DMA

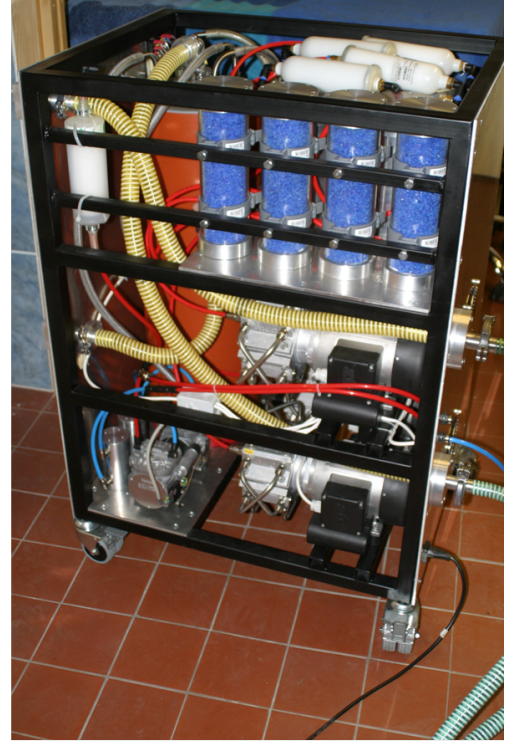


Figure 3.6: Flow Control Unit and Purifying Device

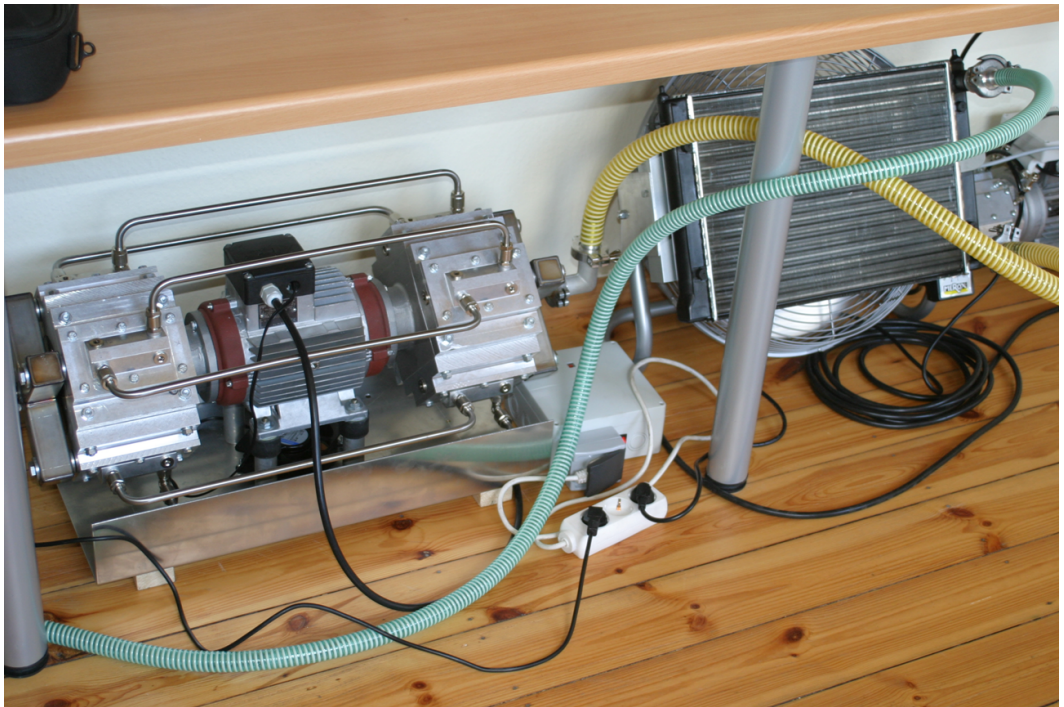


Figure 3.7: 8 Head Membrane Pump and Heat Exchanger

Chapter 4

Experimental Setup

4.1 Electrospray Setup

To become familiar with the electrospray generator the initial steps of the experiments were governed by testing the possible ranges of liquid flow rates, applied high voltage and applied pressure. As the flow rate of the liquid sample depends on its viscosity and the inner diameter of the capillary, the applied pressure has to be adjusted until the liquid reaches the conically shaped tip of the capillary. In a next step, the high voltage applied to the liquid sample is adjusted until a Taylor cone is formed emanating a jet of highly charged liquid droplets. In the literature numerous of different types of Taylor cones have been described, like the multi-jet mode or the single jet mode [34], depending on the applied high voltage and applied pressure. For a stable Taylor cone and sufficiently high concentrations of the generated clusters, the single jet mode turned out to be the most appropriate operation mode in this work. Therefore pressure and high voltage have to be minimized to the lowest values where the Taylor cone is still stable. As already mentioned in chapter 2.1.2 the main advantage of the De la Mora type electrospray and its slightly modified version used during this work is the compact size and the simple way to adjust the operating parameters. Therefore an unstable behavior of the Taylor cone can immediately be corrected by readjusting voltage and/or pressure respectively. Typically the dilution gas flow rate Q_{dil} of purified

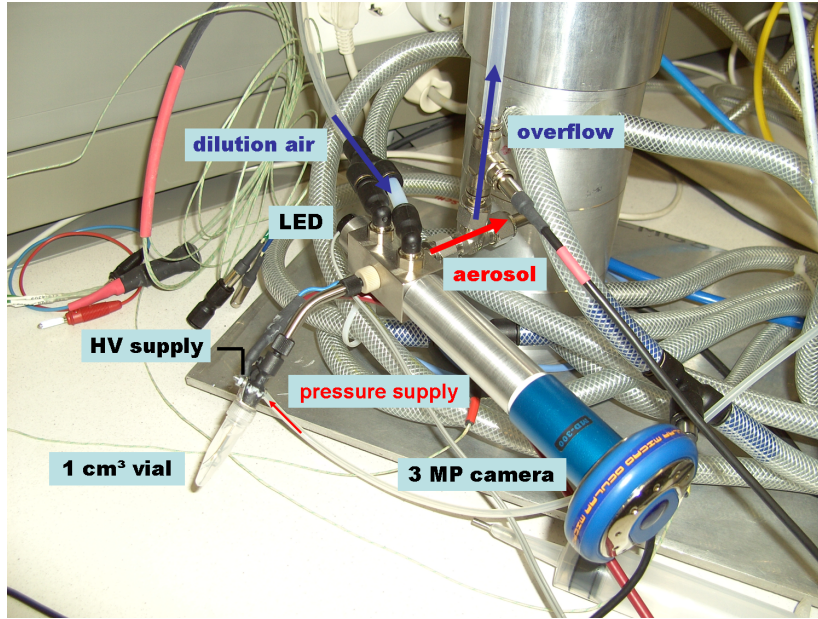


Figure 4.1: Setup with the Vienna Type Electrospay and UDMA

dried pressured laboratory air was adjusted to 17 sl/min. To minimize diffusion losses already in the inlet of the UDMA the electrospay generator is directly flanged to the DMA. As the DMA is operated in a closed loop arrangement where $Q_{sh} = Q_{ex}$ and therefore $Q_a = Q_s$ the aerosol flow rate Q_a is defined by the critical orifice controlled sample air flow Q_s ($Q_s = Q_{fce}$). Typically a sheath air flow rate Q_{sh} of 700 sl/min and aerosol flow rate Q_a of 6.5 sl/min were used. The remaining gas flow from the electrospay is passed through an overflow into an absolute filter and further to an exhaust. The UDMA is connected to a computer controlled process control adjusting the applied voltage to the center electrode. The current corresponding to a certain mobility fraction, extracted by the DMA at a certain voltage is measured in the Faraday Cup Electrometer, amplified and subsequently recorded by the data acquisition software.

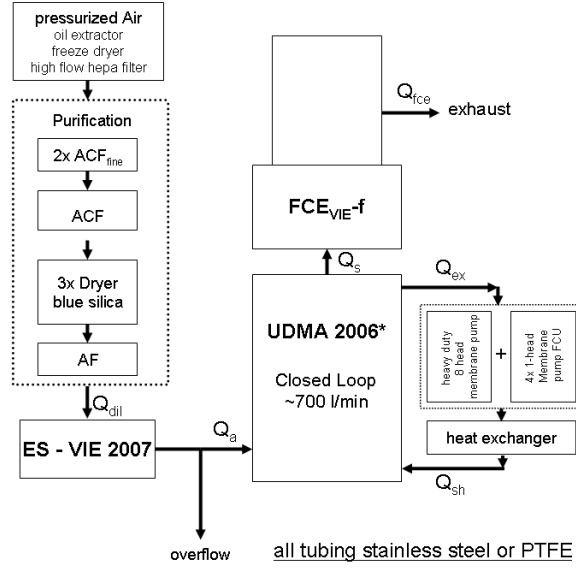


Figure 4.2: Schematic of the Experimental Setup with the Electro spray Generator

4.2 Diffusion Chargers Setup

In this setup the electro spray source is replaced by either an ^{241}Am charger or a unipolar corona charger to investigate the NSD of ionic clusters produced. When used as aerosol neutralizer, the Nt product (product of ion production rate and residence time of the aerosol in the charger) is maintained to be at least 10^7 [35]. However in this study the latter mentioned diffusion chargers are only used as ion cluster sources without the necessity of keeping the Nt product at 10^7 . Therefore flow rates up to 17 sl/min were passed through the chargers to minimize diffusion losses in the ducts to the aerosol inlet port of the EMS. Typically a sheath air flow rate Q_{sh} of 700 sl/min and aerosol flow rate Q_a of 6.5 sl/min were used. The remaining gas flow from the chargers is passed through an overflow into an absolute filter and further to an exhaust.

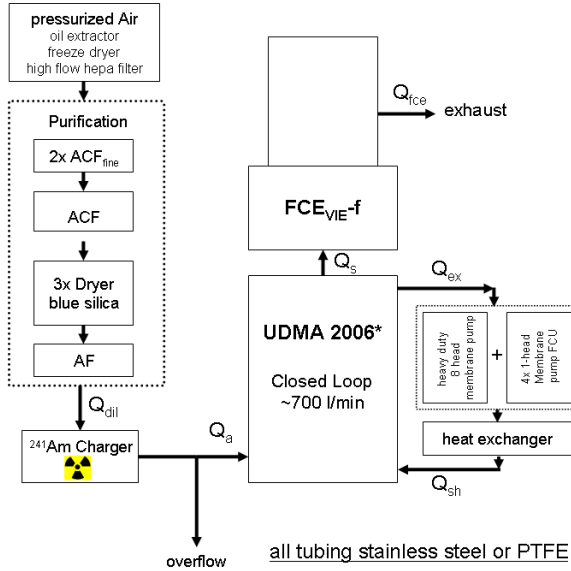


Figure 4.3: Schematic of the Experimental Setup with the Bipolar Diffusion Charger

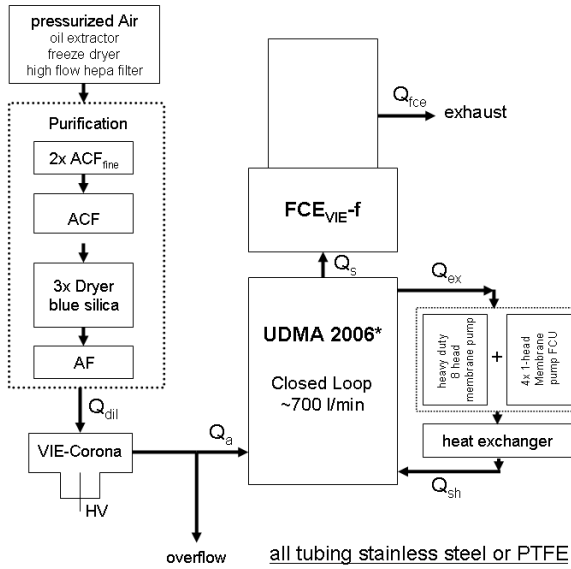


Figure 4.4: Schematic of the experimental Setup with the Corona Charger

Chapter 5

Experimental Results

5.1 Electrospray

5.1.1 Background Measurements

This work focuses on the classification of tetraalkyl halide clusters produced by an electrospray source. Alcohols as Ethanol, Methanol or Isopropanol are well qualified as solvent liquids for the tetraalkyl halides. To determine the background cluster concentration of high grade solvent liquids extensive measurements were performed using pure alcohols as liquid sample.

Figure 5.1 shows the number size distributions of pure Methanol, Ethanol and Isopropanol. The smallest clusters are found for Methanol at 1.1 nm (blue line). Three additional peaks are localized at 1.23 nm, 1.4 nm and 1.48 nm. Ethanol (green line) yields a size distribution of seven peaks at 1.11 nm, 1.24 nm, 1.35 nm, 1.45 nm, 1.57 nm, 1.68 nm and 1.77 nm with its main peak at 1.45 nm. Isopropanol (red line) shows a much less pronounced size distribution with five peaks at 1.34 nm, 1.44nm, 1.54nm, 1.63 nm and 1.7 nm. As Ude and De la Mora [33] presented the spectra of various Tetraalkylammonium halide salts showing a series of sharp peaks associated to clusters of the form $(A^+)_m(AB)_n$, the initial Methanol cluster distribution has been found to be least overlapping with the size spectra of the investigated organic substances

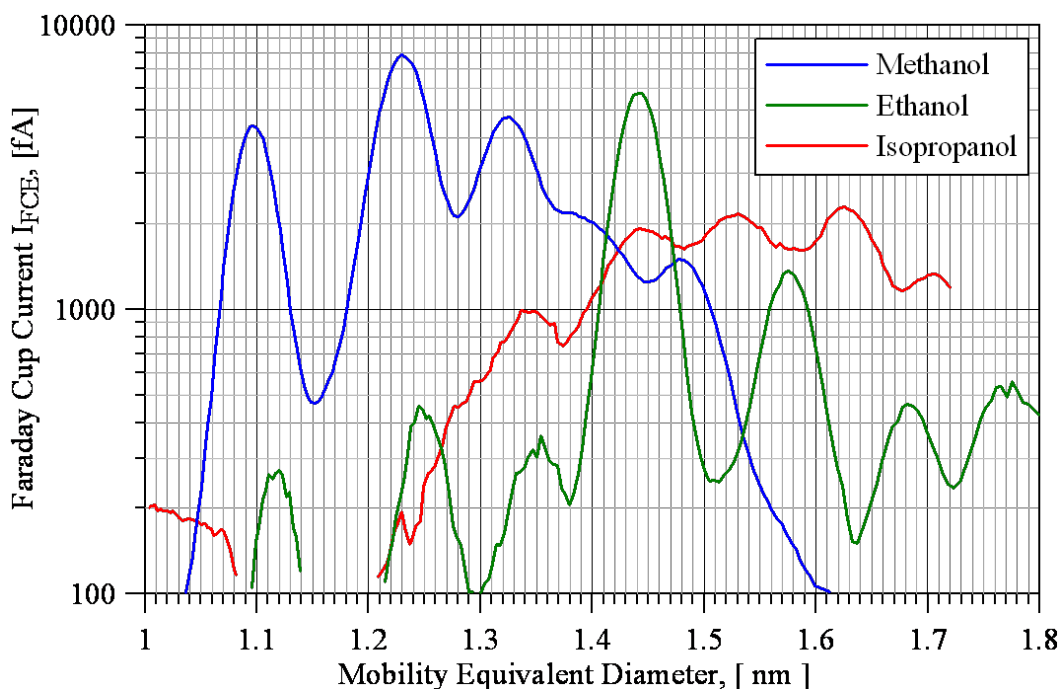


Figure 5.1: NSD of Three Different Pure Alcohols

compared to the other investigated alcohols. Thus high grade Methanol (purity $\geq 99.9\%$, evaporation residue $\leq 0.0005\%$ and water $\leq 0.02\%$) was exclusively used as solvent in the presented experiments.

5.1.2 Tetraheptylammonium Bromide

Figure 5.2 shows the NSD of a 0.3 mMolar Tetraheptylammonium Bromide (THABr) solution. Three sharp peaks corresponding to the monomer (A^+), the dimer ($A+(AB)$) and the trimer ($A+(AB)_2$) at 1.44 nm, 1.77 nm and 1.98 nm are found.

Figures 5.3, 5.4 and 5.5 show a simulation of the possible structure of the THABr ions computed with the ChemOffice ultra software (CambridgeSoft). This program was used for all subsequent simulations too. The dark blue sphere in the center represents the nitrogen atom and the light blue spheres the carbon atoms. The white balls typify the OH molecules and the green ones the Bromide atoms. The Bromide atom carrying a single elementary charge is weakly (ionic) bonded to the residual molecule. Therefore it can easily be separated by electrical stress, leading to a positively charged molecule.

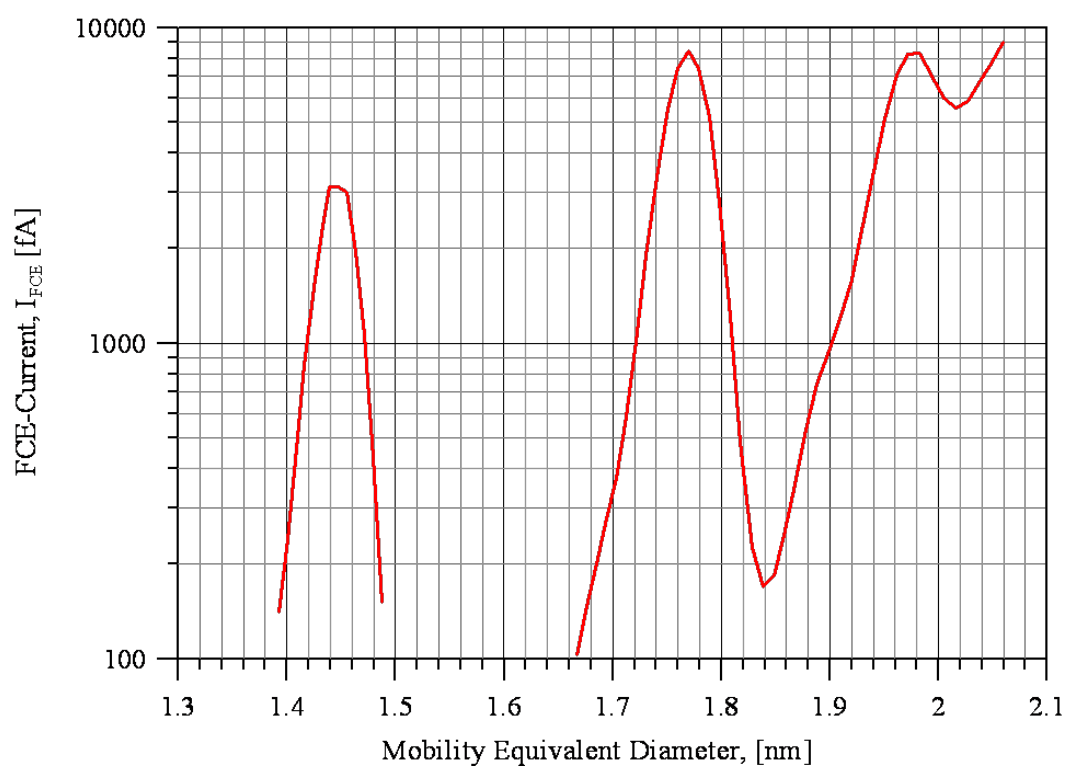


Figure 5.2: NSD of THABr

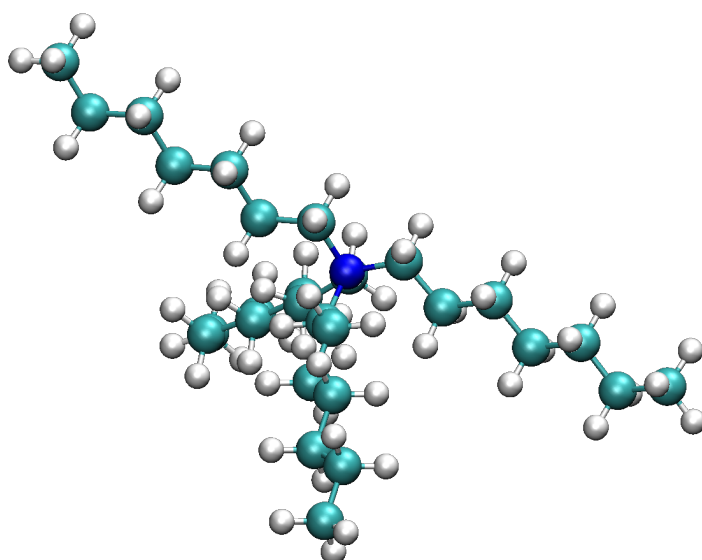


Figure 5.3: Possible Molecular Structure of THA+

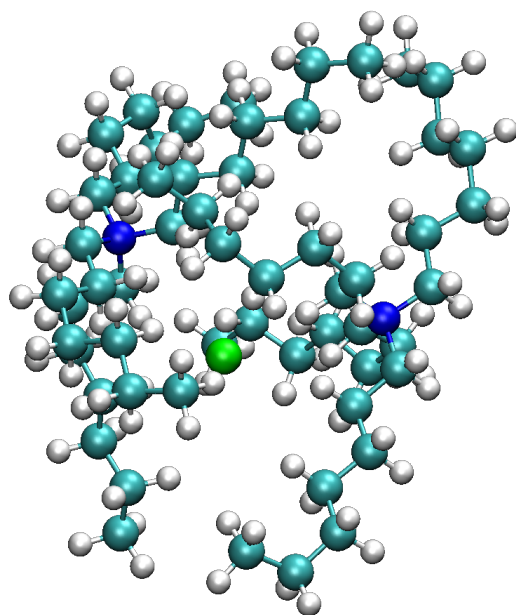


Figure 5.4: THABr Dimer

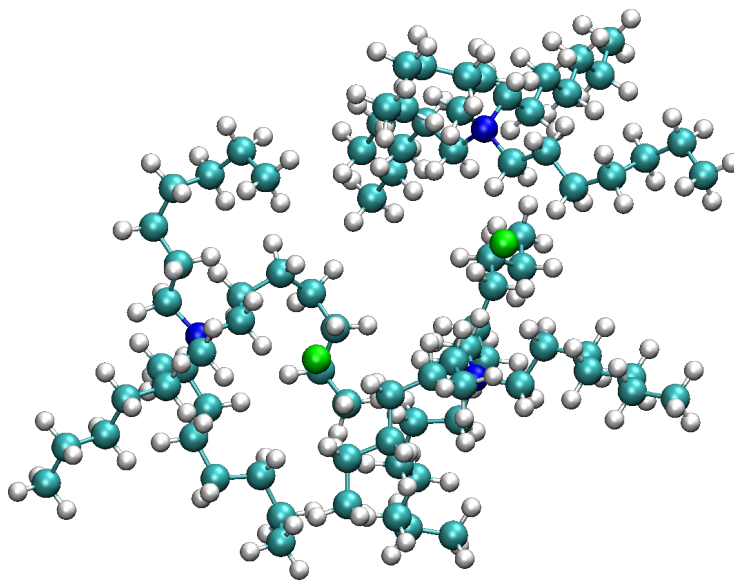


Figure 5.5: THABr Trimer

Figure 5.6 shows a comparison between the measured (blue line) and simulated (red line) transfer function of the UDMA. The transfer function was measured using

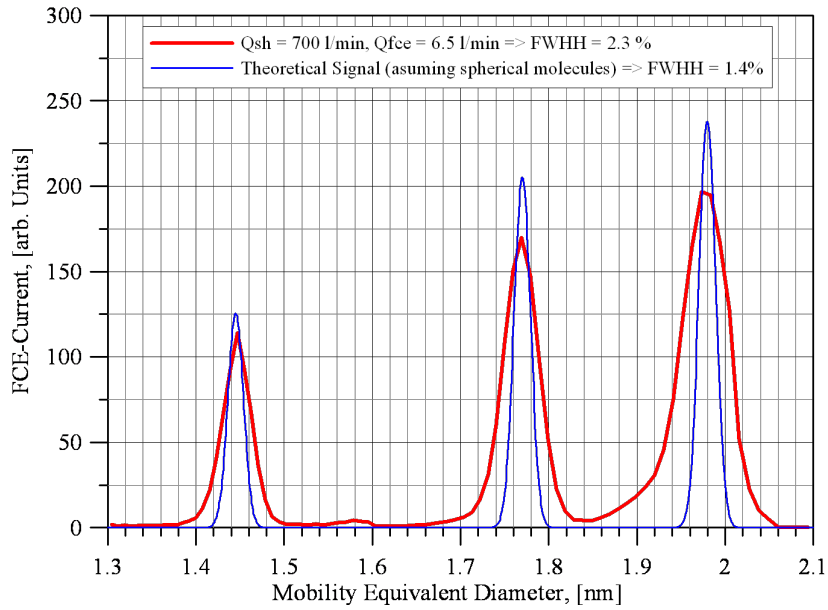


Figure 5.6: Simulated and Measured Transfer Function of the UDMA

THABr as mobility standard.

5.1.3 Tetrabutylammonium Iodide

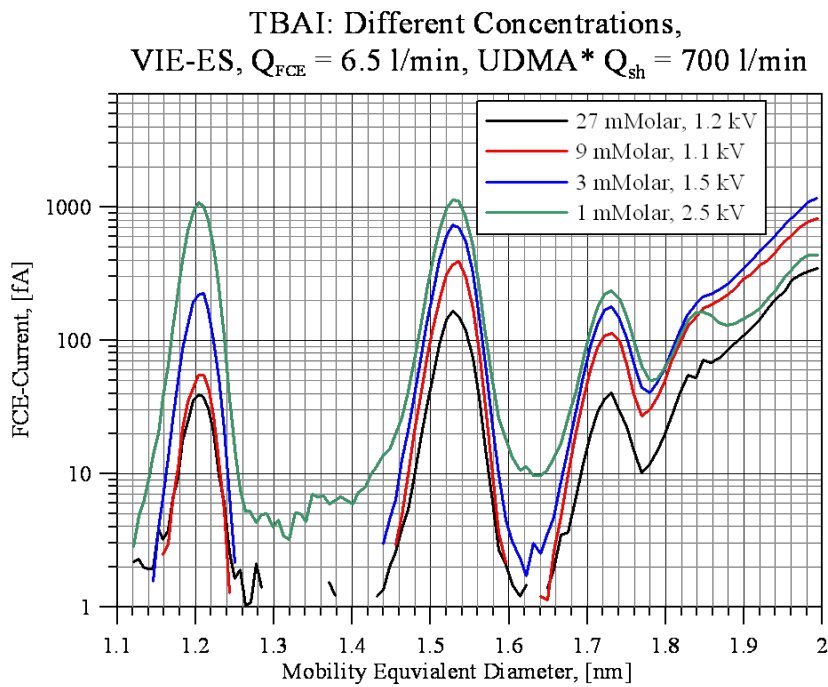


Figure 5.7: NSD of TBAI Molecules

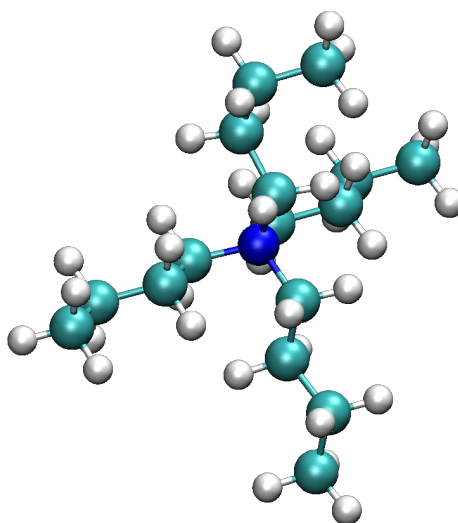


Figure 5.8: Possible Molecular Structure of TBA+

Figure 5.7 shows the NSD of the Tetrabutylammonium Iodide (TBAI) clusters with different concentrations of the dissolved substance at different high voltages applied. The black line shows the NSD of TBAI at a concentration of 27 mM and 1.2 kV, the red line shows a 9 mM concentration at 1.1 kV, the blue line a 3 mM concentration at 1.5 kV and the green line shows a concentration of 1 mM at 2.5 kV. As the butyl chains of TBAI are shorter than the heptyl chains, the TBA⁺ cation (A^+) is found at 1.3 nm, the dimer ($A + AB$) at 1.5 nm and the the trimer ($A + AB$)₂ at 1.7 nm.

Figure 5.8 shows the possible molecular structure of the TBA⁺ cation and figure 5.9 shows the simulated molecular structure of the TBAI⁺ ion. As the Iodide atom, similar to the Bromide atom in the case of the THABr, is weakly bonded to the residual molecule, the same charge transfer process takes place resulting in a overall positively charged molecule.

Figure 5.10 shows the trimer of the TBAI where the dark blue sphere represents the nitrogen atom, the light blue the carbon atoms and the white balls the OH groups. In this case the green sphere represents the Iodide atom.

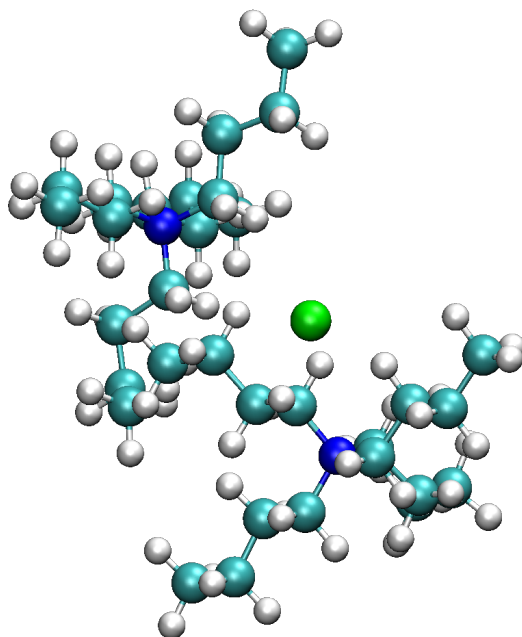


Figure 5.9: Possible Molecular Structure of TBAI Dimer

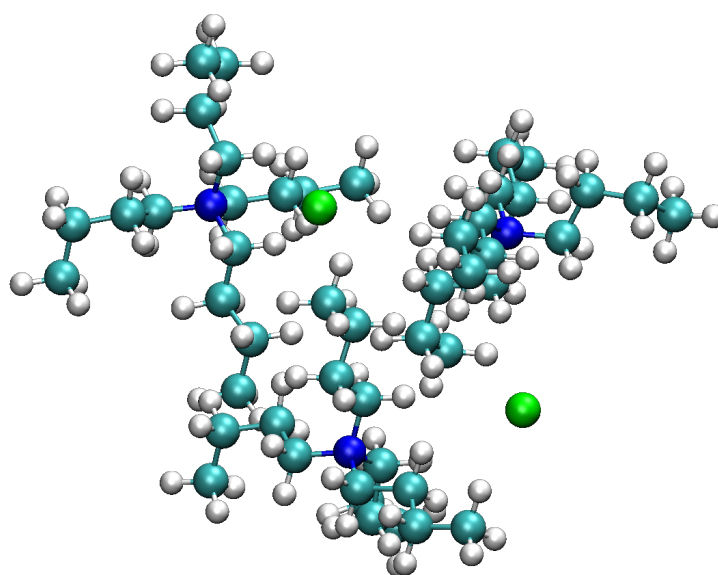


Figure 5.10: Molecular Structure of the TBAI Trimer

5.1.4 Tetrapentylammonium Iodide

Figure 5.11 shows the NSD of the TPtAI molecules with sizes of 1.297 nm for the TPtA⁺ ion, 1.625 nm for the TPtAI ion and 1.81 nm for the trimer. Different con-

TPAI: Different Concentrations,
VIE-ES, $Q_{FCE} = 6.5$ l/min, UDMA* $Q_{sh} = 700$ l/min

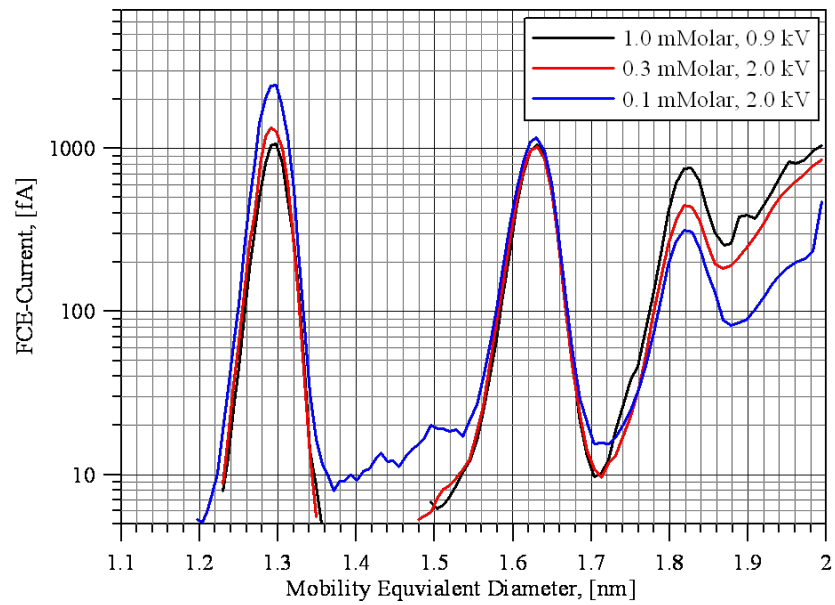


Figure 5.11: NSD of the TPtAI Molecules

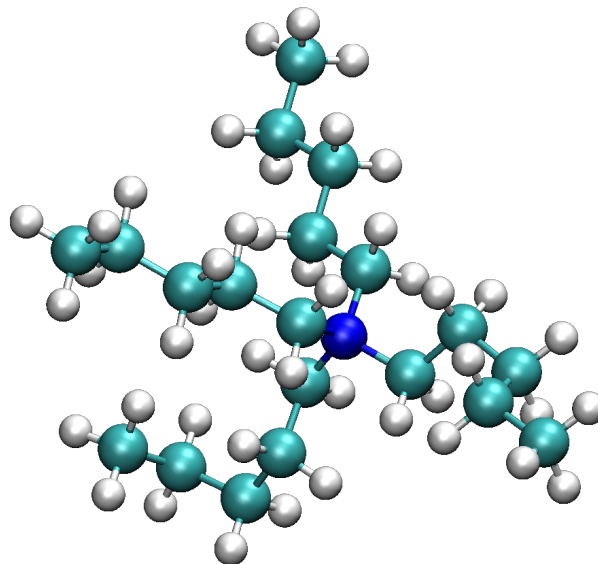


Figure 5.12: TPtAI

centrations of the dissolved substance with different applied high voltages are shown; the black line shows a concentration of 1 mM at +0.9 kV, the red line shows a concentration of 0.3 mM at +2 kV and the blue line shows a concentration of 0.1 mM at +2 kV.

The calculated structures of Tetrapentylammonium Iodide (TPtAI) are shown in figures 5.12, 5.14 and 5.13. As they undergo the same charge transfer process as the molecules presented above, they are overall positively charged too. The alkyl chains of these molecules are slightly longer than those of the organic molecules presented above, resulting in slightly larger mean diameters. The dark blue sphere represents the nitrogen atom, the light blue ball the carbon atoms and the white ones are the OH groups. The green spheres characterize the Bromide atoms.

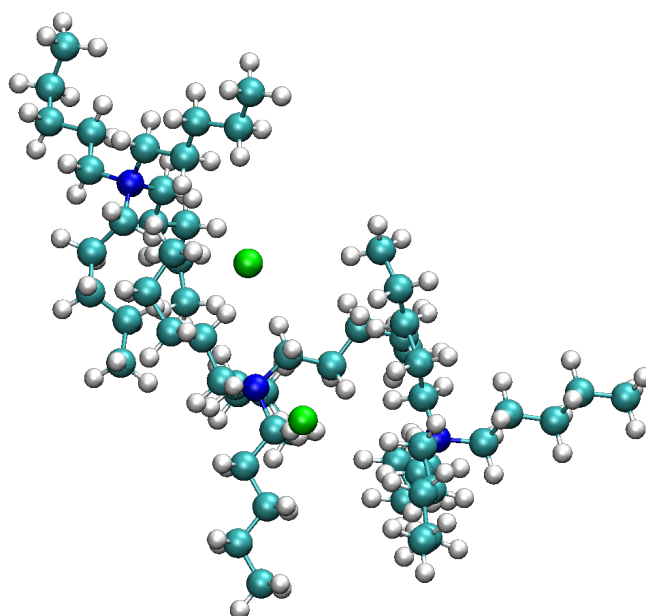


Figure 5.13: Molecular Structure of the TPtAI Trimer

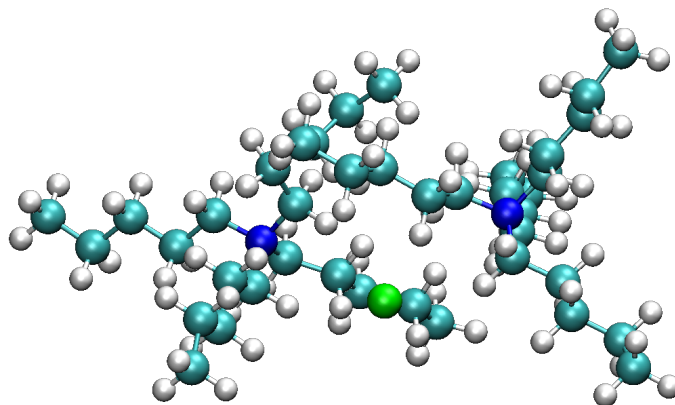


Figure 5.14: Molecular Structure of the TPtAI Trimer

5.1.5 Tetradodecylammonium Bromide

Figure 5.15 shows the NSD for the TDDABr, with a mobility equivalent diameter of 1.69 nm for the TDDA⁺ ion and 2.25 nm for the TDDABr⁺ ion. Different colors of the lines are determined by using different concentrations of the dissolved substance with different values for the applied high voltages. The black line was determined with a 3 mM solution at +1.2 kV, the red line with a 1 mM solution and +1.7 kV, the blue line with a 0.3mM solution and +2.5 kV and the green line with a 0.1 mM solution and a value for the applied voltage of +3 kV. Tetradodecylammonium Bromide (TDDABr) is the molecule with the longest alkyl chains presented in this work. The same charge transfer process takes place as already explained for the THABr molecule. The ionic bonding of the Bromide atom breaks up when exposed to an electrical stress resulting an overall positively charged molecule. Figures 5.16 and 5.17 show the computed molecules, where the dark blue sphere characterizes the nitrogen atom, the light blue balls represent the carbon atoms, the white ones typify the OH groups and the green sphere represents the Bromide atom.

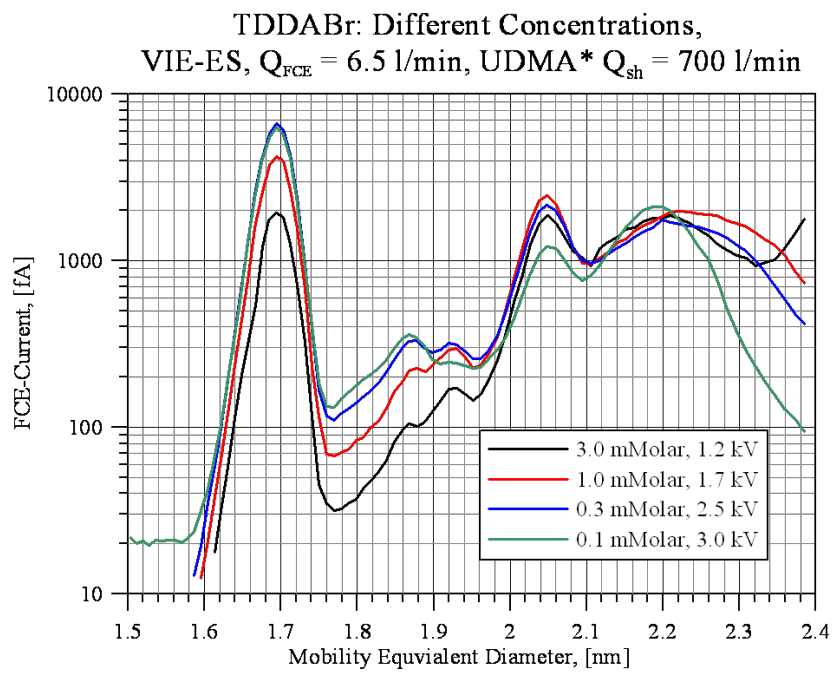


Figure 5.15: NSD of the TDDABr

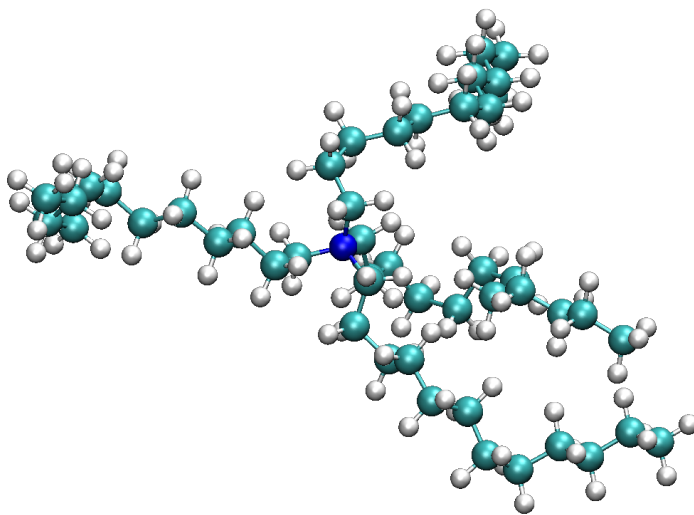


Figure 5.16: Molecular Structure of TDDABr

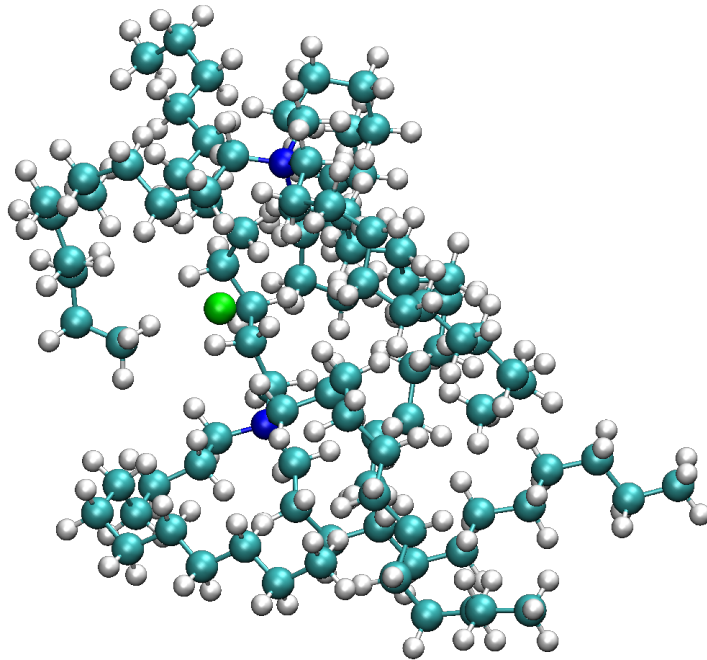


Figure 5.17: Molecular Structure of the TDDABr

5.1.6 Nucleation Experiments

Heterogeneous nucleation experiments, requiring highly monodisperse seed particles, were performed in cooperation with Dr. Paul Winkler, Dr. Paul Wagner, Mag. Gerhard Steiner and Dr. Georg Reischl. To study the particle growth in a supersaturated vapor the Size Analyzing Nuclei Counter (SANC), located at the Faculty of Physics of the University of Vienna was used. In these experiments a well-defined and almost saturated binary n-propanol-air vapor mixture is led into the thermo stated expansion chamber, the core part of the SANC, to achieve the desired vapor saturation prior to expansion. The system is based on computer controlled measurement cycles where the parameters as pressure and temperature after the expansion can be controlled. The chamber is opened to a low pressure buffer tank by a fast large size expansion valve, resulting in an adiabatic expansion with variable expansion times (typically 8-12 ms). The seed particles lead to heterogeneous vapor nucleation and furthermore to a formation and subsequent growth of liquid droplets. Using the Constant Angle Mie

Scattering Method (CAMS) [36], the radius and number concentration of the growing droplets can be determined simultaneously at various times during the growth process without any external calibration. Therefore the growing particles in the expansion chamber are illuminated by a laser beam and the scattered light flux as well as the transmitted light flux are measured. The normalized scattered light flux versus the time curves can be compared with the theoretical light fluxes calculated with the Mie theory. This comparison reveals size and number concentration of the growing droplets. As the electro spray used throughout this work proved to provide well-defined monomobile Tetraalkyl ammonium halide clusters, the latter was used as seed particle source for the above mentioned nucleation experiments. Figure 5.18 shows a schematic of the setup with the SANC and the electro spray generator. In the course of preparing the above mentioned experiments, the electro spray was operated during long time period performance tests to analyze the time stability of the generated cluster concentrations. The operating parameters (voltage, pressure, solvent concentration) were optimized to achieve sufficient high concentrations for the specific cluster species classified by the UDMA at a sheath air flow rate Q_{sh} of approx. 536 sl/min and aerosol flow rate Q_a of 6.5 sl/min.

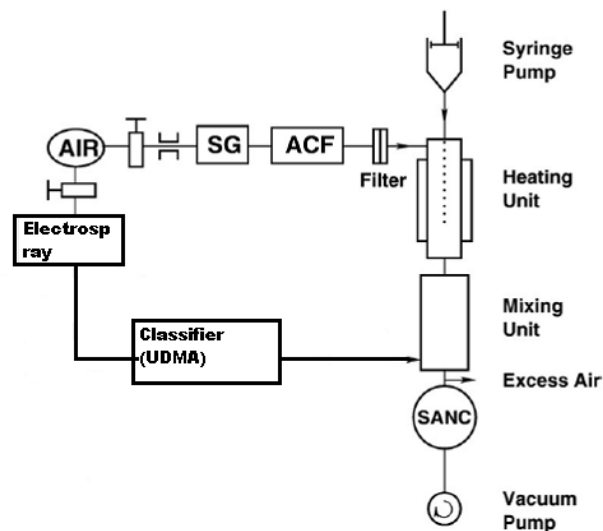


Figure 5.18: Schematic of the Experimental Setup for the Nucleation Experiments

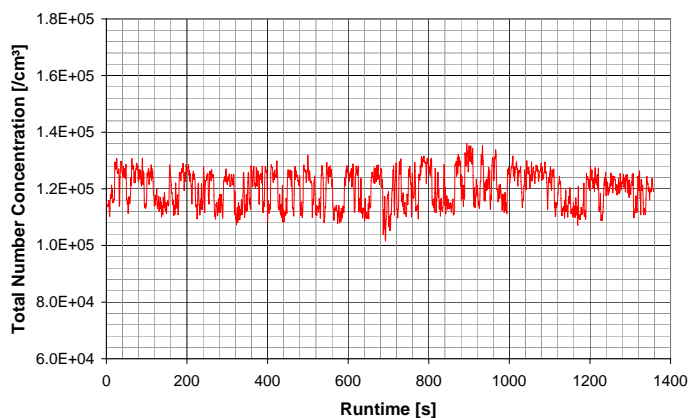


Figure 5.19: Particle concentration of the TDDA⁺ cation, classified at a DMA voltage of approx. 950 V, in a 0.8 mMolar solution, versus electrospray generator runtime. The applied high voltage potential to the liquid sample was +2.8 kV.

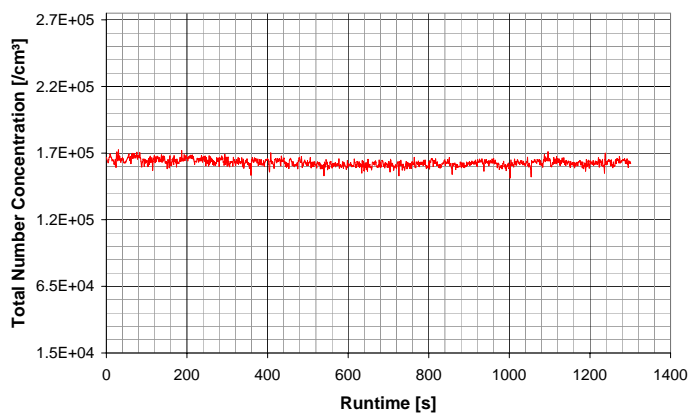


Figure 5.20: Particle concentration of the TDDABr⁺ ion, classified at a DMA voltage of approx. 1400 V, in a 0.8 mMolar solution, versus electrospray generator runtime. The applied high voltage potential to the liquid sample was +2.8 kV.

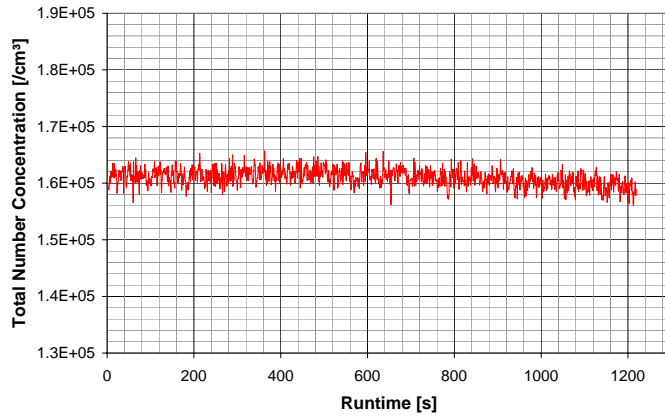


Figure 5.21: Particle concentration of the TPtAl⁺ cation, classified at a DMA voltage of approx. 550 V, in a 0.05 mMolar solution, versus electrospray generator runtime. The applied high voltage potential to the liquid sample was +2.3 kV.

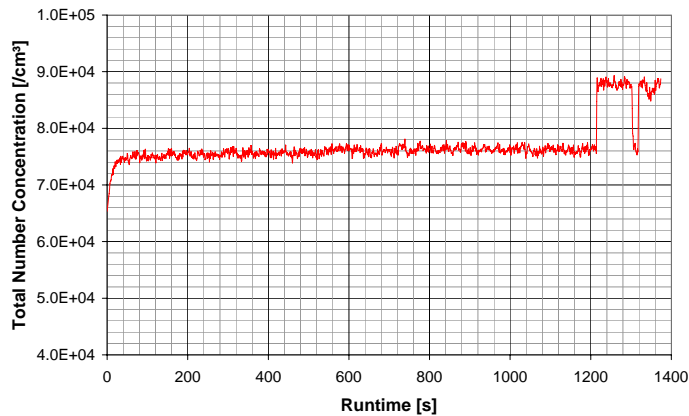


Figure 5.22: Particle concentration of the TPtAl⁺ ion, classified at a DMA voltage of approx. 1950 V, in a 0.05 mMolar solution, versus electrospray runtime. The applied high voltage potential to the liquid sample was +2.3 kV. At 1213 seconds the main concentration increases as the high voltage potential was decreased to +2.0 kV.

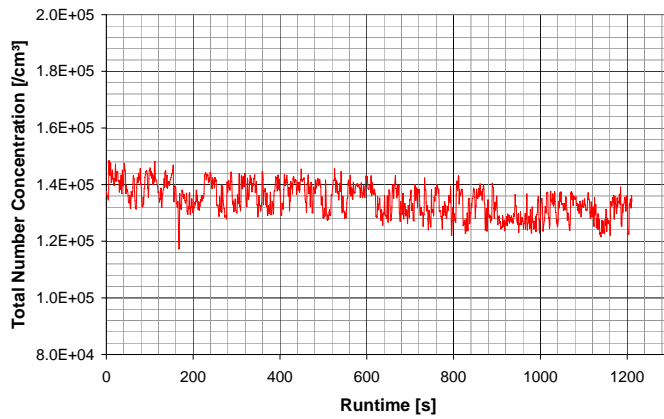


Figure 5.23: Particle concentration of the THA⁺ cation, classified at a DMA voltage of approx. 690 V, in a 0.2 mMolar solution, versus electrospray runtime. The applied high voltage to the liquid sample was +2.8 kV.

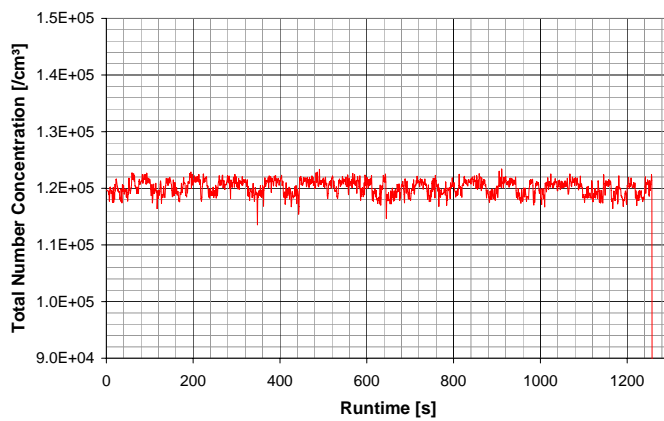


Figure 5.24: Particle concentration of the THABr⁺ ion, classified at a DMA voltage of approximately 1030 V, in a 0.2 mMolar solution, versus electrospray runtime. The applied high voltage to the liquid sample was +2.8 kV.

5.2 Ion Cluster Sources

5.2.1 Diffusion Charger Ions

As already described in chapter 3.1 the EMS method is based on the classification of charged particles. Widely used methods to charge and/or neutralize aerosol particles is bipolar diffusion charging by radioactive sources and unipolar diffusion charging by corona discharge. As already described in chapter 2.5, in both methods gas molecules are first ionized by an ionizing radiation forming primary ions which subsequently combine with polar molecules present in the carrier gas to build larger ionic clusters. As can be seen in figures 5.25 and 5.26 negative and positive ions produced by the above mentioned mechanisms, form a spectrum of different cluster species closely situated to each other. The black diamonds in the following figures represent the NSD of ions produced by corona discharge. The red dots refer to the NSD of ions produced by an ^{241}Am charger.

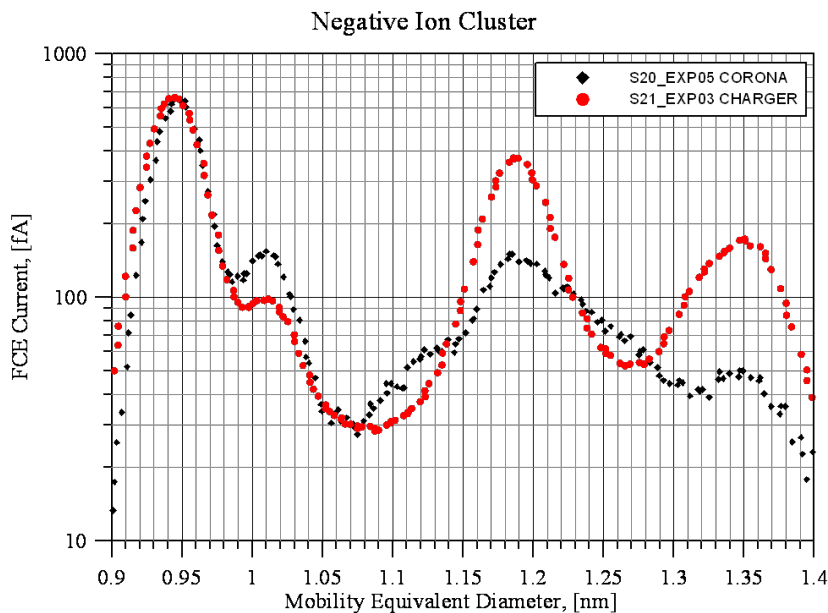


Figure 5.25: NSD of Negative Ion Clusters

For the negative ionic clusters peaks at 0.945 nm, 1.01 nm, 1.19 nm and 1.35 nm where the 0.945 nm peak is predominant were found. Positive ionic clusters are

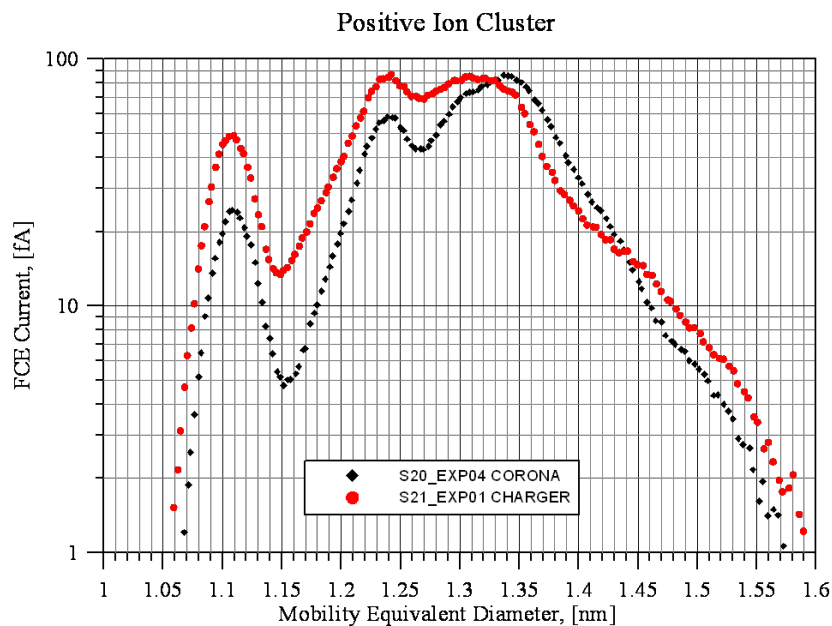


Figure 5.26: NSD of Positive Ion Clusters

located at 1.11 nm, 1.24 nm, 1.31 nm and 1.34 nm. The species of the clusters formed by different mechanisms seem to be the same. Only their relative concentrations vary depending on the generating mechanism as well as on the operation conditions. This indicates a very similar cluster formation process. As water molecules are the most likely present polar molecules in the purified air, it is assumed that the formed ionic clusters are built by n -fold hydration of the primary ions [7]. The experiments show that the pattern of the NSD of the negative ionic clusters observed is slightly shifted toward smaller sizes compared to the NSD of positive clusters, indicating lower hydration states of the negative ions.

5.2.2 Electro sprayed Water Clusters

To clarify the role of water in the cluster formation process, additional investigations were carried out using high grade purified water (< 5 ppm non-volatile residues) as liquid sample for electrospray experiments. As the conductivity of pure water is very low, the applied voltage has to be slightly larger compared to the voltages used for the solutions presented before (e.g. THABr) and it is more difficult to achieve a

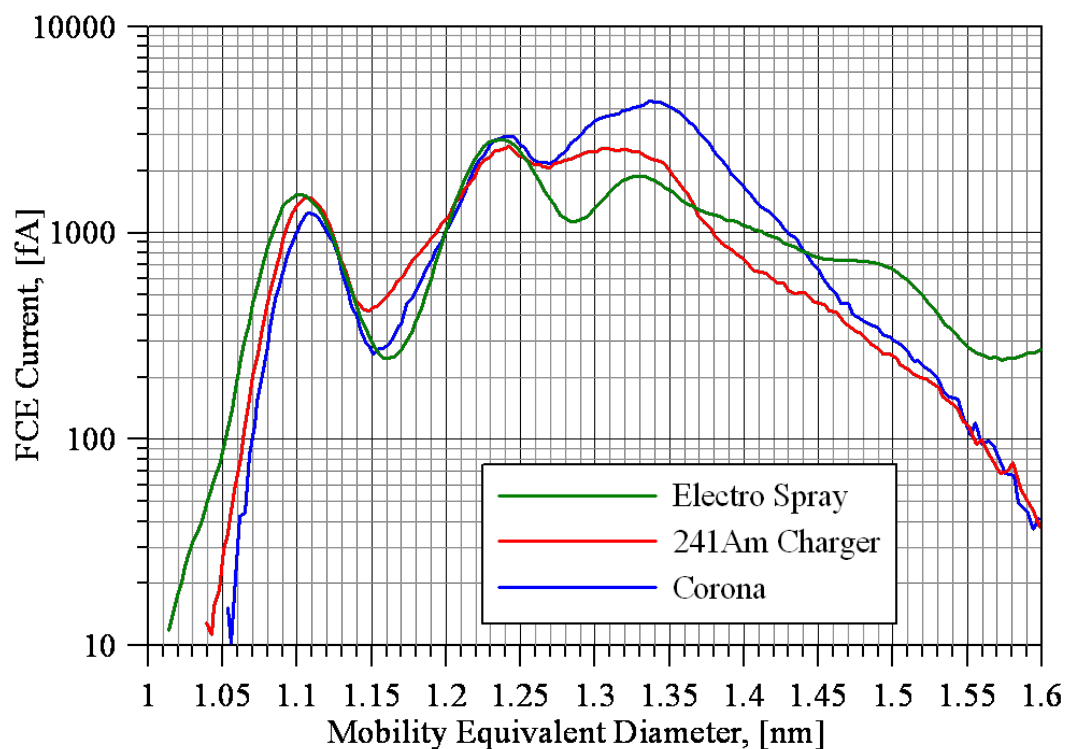


Figure 5.27: Comparison of Different Positive Ion Clusters

stable Taylor cone and cluster concentration. A comparison of positively charged water clusters produced by the three discussed mechanisms is shown in figure 5.27. An identical pattern of NSDs with peaks at 1.11 nm, 1.24 nm, 1.31nm and 1.34 nm, again only varying in the relative concentrations of the cluster species was observed. Corona discharge cannot be completely discarded as source of the ions observed from the electrospray of water. However the typical ion size distribution produced by corona discharge was never observed during the experiments with the Tetraalkyl ammonium halides at even higher voltages applied to the liquid sample.

Chapter 6

Discussion

6.1 Feasibility of the Electrospray

As already mentioned in chapter 3.1 high resolution DMAs operating at extraordinary high flow rates up to several m^3/min require calibration. Therefore well-defined mobility standards that can easily be reproduced are of crucial importance. In this work it is shown that the electrospray generator is able to cover the above mentioned experimental needs using various Tetraalkyl ammonium halide salts dissolved in high grade alcohols. As the NSDs of the electrosprayed solutions of these substances show several uniquely identifiable monomobile cluster species, they are well qualified for numerous applications in aerosol science. Especially in combination with a high resolution classifier it is a perfect tool for studies where high quality monodispersed particles are of crucial importance. Further this method has proved long time period stability of generated cluster concentrations. In this work, only singly charged clusters were investigated. However the generation method also allows to provide multiply charged monomolecular clusters of well-defined sizes [37].

6.2 Kilpatrick's mass-mobility Relationship

An estimation of the mobility equivalent diameter from the molecular mass can be determined by using the empirical correlation between the mass number and the mobility, described by Kilpatrick [38]. J. Mäkelä (personal communication) suggested an analytical function describing this correlation in a good approximation:

$$M = \exp[A \cdot (\ln(Z))^2 + B \cdot \ln Z + C]$$

with $A = -0.4264$, $B = -2.263$ and $C = 6.008$. This function can be inverted and hence with a known mass number M , the corresponding mobility Z_0 (at $p_0 = 760\text{mmHg}$ and $t_0 = 0^\circ\text{C}$) can be determined:

$$Z_0 = \exp \left[\frac{1}{2 \cdot A} \cdot (\sqrt{(B^2 - 4 \cdot A \cdot C) + 4 \cdot A \ln M} - B) \right]$$

At experimental conditions (p,t) the mobility $Z_{p,t}$ can be determined with Z_0 as follows:

$$Z_{p,t} = Z_0 \cdot \frac{p_0}{p} \cdot \frac{273.15 + t}{273.15}$$

and the corresponding mobility equivalent diameter, by inverting numerical the defining equation for the electrical mobility:

$$Z = \frac{1 \cdot e_0 \cdot C(\overline{D_p})}{3 \cdot \pi \cdot \eta \cdot \overline{D_p}}$$

If the species of the ion clusters and therefore its mass is known, it will be possible to correlate its measured electrical mobility to its mass and further reevaluate Kilpatrick's empirical relationship.

A section of the fit of this relation for very high mobilities is shown in figure 6.1. It can be transferred into a relation between mass and mobility equivalent diameter as well (see figure 6.2). Figure 6.3 shows a comparison between the measured electrical mobilities versus the known ionic cluster masses of various selected Tetraalkyl ammonium halide salts and Kilpatrick's empirical mass-mobility relation. In general the measured points correlate quite well with Kilpatrick's empirical relation. However especially for small ionic clusters the measured mobility is found to be significantly larger

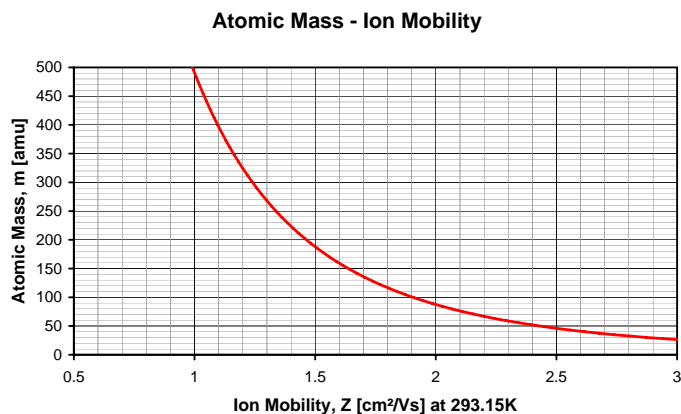


Figure 6.1: Mäkelä Fit for Kilpatrick's Mass-Mobility Relation

than predicted according to their mass by Kilpatrick. Most of the shown mobilities have been measured by Ude & de la Mora. During this work numerous measurements of the mobility spectra of Tetraalkyl ammonium halide salts have been performed (chapter 5.1) and were found to agree with the mobilities measured by Ude & de la Mora.

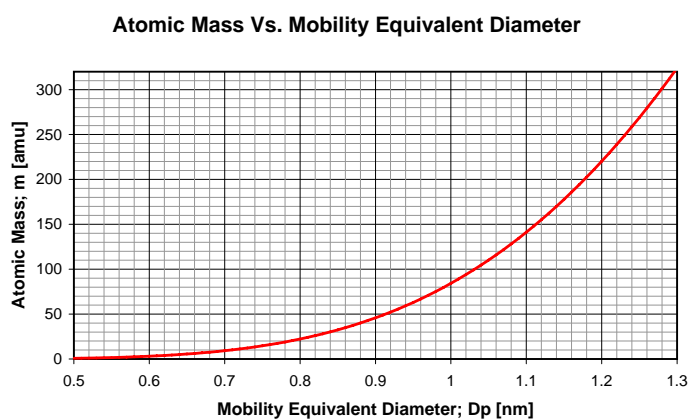


Figure 6.2: Atomic Mass vs. Mobility Equivalent Diameter according to Kilpatrick's Relation

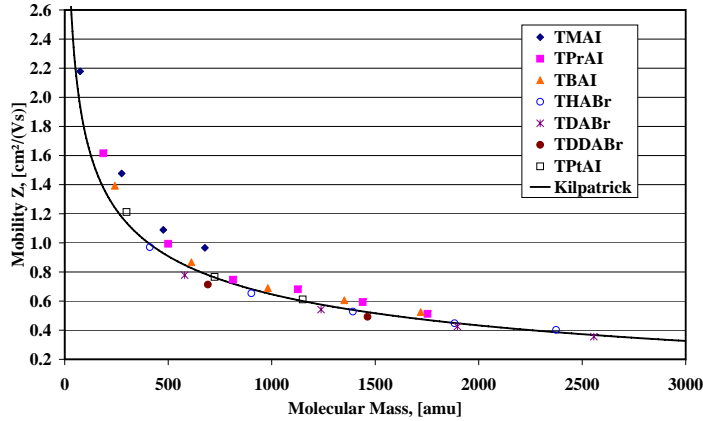


Figure 6.3: Mass versus Electrical Mobility of Tetraalkyl Ammonium Haldies (TMAI = Tetramethyl ammonium Iodide, TPrAI = Tetrapropyl Ammonium Iodide, TBAI = Tetrabutyl Ammonium Iodide, THABr = Tetraheptyl Ammonium Bromide, TDABr = Tetradecyl Ammonium Bromide, TDDABr = Tetradodecyl Ammonium Bromide and TPtAI = Tetrapentyl Ammonium Iodide).

6.3 Corona Discharge from Electrospray

As mentioned in chapter 5.2.2 the role of water in the cluster formation process of diffusion chargers is still an open question. The results of the electrospray measurements of water as liquid sample seem to strongly support the hypothesis of water as predominant partner in the formation of ionic clusters. However the presented results have to be reevaluated due to the fact that a corona discharge cannot be discarded and therefore has to be avoided in future experiments.

Curriculum Vitae

Name: Daniela Wimmer

Date of birth: April 4th, 1984

Place of birth: Vienna

Nationality: Austria

Marital status: single

1994-2002: Gymnasium AHS Sacré-Coeur, Vienna

June 2002: Matura

since 2002: Diploma study of *physics* at the University of Vienna

since September 2006: Diploma thesis in Aerosol, Bio- and Environmental Physics,
Faculty of Physics, University of Vienna (supervisor: Prof. Georg Reischl):
Generation and Classification of Airborne Molecular Clusters

Lebenslauf

Name: Daniela Wimmer

Geburtsdatum: 4. April 1984

Geburtsort: Wien

Staatsbürgerschaft: Österreich

Familienstand: ledig

1994-2002: Gymnasium AHS Sacré-Coeur, Wien

Juni 2002: Matura

seit 2002: Studium *Physik Diplom* an der Universität Wien

seit September 2008: Diplomarbeit in der Aerosol, Bio- und Umweltphysik - Gruppe,
Fakultät für Physik, Universität Wien (Betreuer: Prof. Georg Reischl) mit dem
Thema:

Generierung und Klassifizierung gasgetragener molekularer Cluster

Bibliography

- [1] J. M. H. Peters. Rayleigh's electrified water drops. *European Journal of Physics*, 1:143 – 146, 1980.
- [2] Lord Rayleigh. *The Theory of Sound*. PhD thesis, Dover, New York, 1945.
- [3] Lord Rayleigh. On the equilibrium of conducting masses charged with electricity. Master's thesis, 1882.
- [4] De La Mora J.F. Rosell-Llompart J. Generation of monodisperse droplets 0.3 to 4 μm in diameter from electrified cone-jets of highly conducting and viscous liquids. *Journal of Aerosol Science*, 25, Issue 6:1093 – 1119, 1994.
- [5] Colhoun M. Enderle K.H. Gras J. Julanov Yu Kaller D. Lindner A. Lushnikov A.A. Mavliev R. McGovern F. O'Connor T.C. Podzimek J. Preining O. Reischl G.P. Rudolf R. Sem G.J. Szymanski W.W. Vrtala A.E. Wagner P.E. Winklmayr W. Zagaynov V. Ankilov A., Baklanov A. Particle size dependent response of aerosol counters. *Atmospheric Research*, 62(3-4):209 – 237, 2002.
- [6] Neced J. Reischl G.P., Mäkelä J.M. Performance of vienna type differential mobility analyzer at 1.2-20 nanometer. *Aerosol Science and Technology*, 27, Issue 6:651 – 672, 1997.
- [7] Gerhard Steiner. Generierung von nanopartikel - Über die konstruktion eines wolfram oxid heizdraht generators. Master's thesis, University of Vienna, Faculty of Physics, 2006.

- [8] Reischl G. P. Wimmer D. Sippilä M. Kulmala M. Steiner G., Attoui M. High resolution mobility measurement of ionic molecular clusters. In *European Aerosol Conference, Thessaloniki*, 2008.
- [9] Schmidt-Ott A. Peineke C., Attoui M.B. Using a glowing wire generator for production of charged, uniformly sized nanoparticles at high concentrations. *Journal of Aerosol Science*, 37, Issue 12:1651 – 1661, 2006.
- [10] Schmidt-Ott A. Schwyn S., Garwin E. Aerosol generation by spark discharge. *Journal of Aerosol Science*, 19, Issue 5:639–642, 1988.
- [11] Tabrizi N. Schmidt-Ott A. Kelder E. M. Simonin L., Lafont U. Sb/o nanocomposites produced via spark discharge generation for li-ion battery anodes. *Journal of Power Sources*, 174:805–809, 2007.
- [12] Koffer F. Wadenpohl C. Kaufman Stanley L. Wenninger G. Helsper C., Molter W. Investigations of a new aerosol generator for the production of carbon aggregate particles. *Atmospheric Environment part A-General Topics*, 27, Issue 8:1271–1275, 1993.
- [13] Gangl M. Horvath H. A low-voltage spark generator for production of carbon particles. *Journal of Aerosol Science*, 34, Issue 11:1581–1588, 2003.
- [14] M.B. Attoui. Characterisation of the spark generator in the nanometric range. In *European Aerosol Conference, Thessaloniki, Abstract T01A028P*, 2008.
- [15] de La Mora J. F. Attoui M.B. A dma covering the 1-100 nm particle size range with high resolution down to 1 nm. In *European Aerosol Conference, Salzburg, Abstract T09A029*, 2007.
- [16] N. A. Fuchs. *The Mechanics of Aerosols*. Pergamon Press, Oxford, 1964.
- [17] H. Rohmann. Methode zur messung der groeße von schwebeteilchen. *Zeitschrift fuer Physik*, 17:253, 1923.

- [18] Whitby K. T. Knutson E. O. Aerosol classification by electric mobility -apparatus, theory and applications. *Journal of Aerosol Science*, 6:443, 1975.
- [19] Whitby K. T. Knutson E. O. Accurate measurement of aerosol electric mobility moments. *Journal of Aerosol Science*, 6:453, 1975.
- [20] G. W. Hewitt. The charging of small particles for electrostatic precipitation. *Transactions of the American Institute of Electrical Engineers*, 76:294, 1957.
- [21] G.P. Reischl. Measurement of ambient aerosols by the differential mobility analyzer method: Concepts and realization criteria for the size range between 2 and 500 nm. *Aerosol Science and Technology*, 14, Issue 1:5 – 24, 1991.
- [22] Lindner A.O. Berner A. Winklmayr W., Reischl G.P. New electromobility spectrometer for the measurement of aerosol size distributions in the size range from 1 to 1000 nm. *Journal of Aerosol Science*, 22, Issue 3:2889 – 2296, 1991.
- [23] Pourprix M. Renoux A. Mesbah B., Bouland D. Circular electric mobility spectrometer. *Journal of Aerosol Science*, 24:219, 1993.
- [24] Bouland D. Pourprix M. Renoux A. Ooghe M., Mesbah B. Radial flow differential mobility analyzer (rf-dma). In *Proceeding of the 4th International Aerosol Conference, Los Angeles*, pages 463–464, 1994.
- [25] Russell L. M. Flagan R.C. Seinfeld J.H. Zhang S. H., Akutsu Y. Radial differential mobility analyzer. *Aerosol Science and Technology*, 23:357, 1995.
- [26] Seinfeld J.H. Zhang S. H., Flagan R.C. Resolution of the radial differential mobility analyzer. *Journal of Aerosol Science*, 27:1179, 1996.
- [27] M.R. Stoltzenburg. *An ultrafine aerosol size distribution measuring system*. PhD thesis, University of Minnesota, 1988.

- [28] de La Mora J. F. de Juan L. High resolution size analysis of nanoparticles and ions: Running a vienna dma of near optimal length at reynolds numbers up to 5000. *Journal of Aerosol Science*, 29, Issue 5-6:617 – 626, 1998.
- [29] Bingham D. de la Mora J.F. Rosell-Llompart J., Loscertales I.G. Sizing nanoparticles and ions with a short differential mobility analyzer. *Journal of Aerosol Science*, 27, Issue 5:695 – 719, 1996.
- [30] T. Eichler. *A differential Mobility Analyzer for ions and nanoparticles: Laminar flow at high Reynolds numbes*. PhD thesis, Fachhochschule Offenburg, Germany, 1997.
- [31] Bernardo N. de la Mora J.F. Hermann W., Eichler T. Turbulent transition arises at reynolds numbers 35.000 in a short vienna type dma with a large laminarization inlet. In *Annual Conference of the AAAR, St Loius, Missouri*, 2000.
- [32] de la Mora J.F. Rosser S. Vienna-type dma of high resolution and high flow rate. *Aerosol Science and Technology*, 39, Issue 12:1191 – 1200, 2005.
- [33] de la Mora J.F. Ude S. Molecular monodisperse mobility and mass standards from electrosprays of tetra-alkyl ammonium halides. *Journal of Aerosol Science*, 36:1224 – 1237, 2005.
- [34] Prunet-Foch B Cloupeau M. Electrohydrodynamic spraying functioning modes: A critical review. *Journal of Aerosol Science*, 25, Issue 6:1021 – 1036, 1994.
- [35] Pui D.Y.H. Liu B.Y.H. Equilibrium bipolar charge-distribution of aerosols. *Journal of Colloid and Interface Science*, 49, Issue 2:305–312, 1974.
- [36] P. E. Wagner. A constant angle mie scattering method (cams) for investigation of particle formation process. *Journal of Colloid and Interface Science*, 105:Issue 2, 456–467, 1985.

- [37] Lehtipalo K. Neitola K. Steiner G. Kulmala M. Attoui M.B., Sipilä M. Generation of monodisperse and multicharged sub 10 nm peg particles. In *European Aerosol Conference, Thessaloniki, T01A0090*, 2008.
- [38] W. D. Kilpatrick. An experimental mass-mobility relation for ions in air at atmospheric pressure. In *Proceeding of the 19th annual Conference of Mass Spectrometry*, volume 19, pages 320–326, 1971.

List of Figures

2.1	Rayleigh Limit in Dependence of Diameter for Water (blue line) and Alcohols (red line)	14
2.2	Schematic of the Ion Formation Process	15
2.3	Viewing Part of the Fernández de la Mora Electrospray	16
2.4	Schematic of an Electrospray	17
2.5	Closeup of the interior of the Electrospray chamber. It shows the conical tip of the capillary and the liquid jet emanating from the triangular shaped Taylor cone.	18
2.6	Picture of the slightly modified Electrospray Generator	18
2.7	Schematic of the WO_x Generator's Heating Zone	19
2.8	Evolution of the WO_x Generator, a shows the Novosibirsk type built at the Institute of Combustion, b shows the Vienna prototype, built at the University of Vienna and c shows the commercially available 7.680 tungsten oxide generator	20
2.9	Schematic of the Glowing Wire Generator [9]	21
2.10	Glowing Wire Generator Working	22
2.11	Picture of the Glowing Wire Generator	22
2.12	Insight of the Spark Generator	23
2.13	Spark Generator	24
2.14	Control Device for the Spark Generator	25
2.15	High Voltage Supply for the SPG	25
2.16	Schematic of the Spark Generator [13]	26

2.17	Sketch of a Bipolar Am-241 Charger	27
2.18	Unipolar Corona Charger	28
3.1	Transfer Function of the DMA Tr(Z) in case of: $Q_a = Q_s, Q_{sh} = Q_{ex}$. .	32
3.2	Laminarization Sponge	33
3.3	Sketch of the UDMA 2006	34
3.4	UDMA 2006 and Faraday Cup Electrometer	35
3.5	Schematic of a Cylindrical DMA	36
3.6	Flow Control Unit and Purifying Device	37
3.7	8 Head Membrane Pump and Heat Exchanger	37
4.1	Setup with the Vienna Type Electrospray and UDMA	39
4.2	Schematic of the Experimental Setup with the Electrospray Generator .	40
4.3	Schematic of the Experimental Setup with the Bipolar Diffusion Charger	41
4.4	Schematic of the experimental Setup with the Corona Charger	41
5.1	NSD of Three Different Pure Alcohols	43
5.2	NSD of THABr	44
5.3	Possible Molecular Structure of THA+	44
5.4	THABr Dimer	45
5.5	THABr Trimer	45
5.6	Simulated and Measured Transfer Function of the UDMA	46
5.7	NSD of TBAI Molecules	46
5.8	Possible Molecular Structure of TBA+	47
5.9	Possible Molecular Structure of TBAI Dimer	48
5.10	Molecular Structure of the TBAI Trimer	48
5.11	NSD of the TPtAI Molecules	49
5.12	TPtAI	49
5.13	Molecular Structure of the TPtAI Trimer	50
5.14	Molecular Structure of the TPtAI Trimer	51
5.15	NSD of the TDDABr	52

5.16	Molecular Structure of TDDABr	52
5.17	Molecular Structure of the TDDABr	53
5.18	Schematic of the Experimental Setup for the Nucleation Experiments .	54
5.19	Particle concentration of the TDDA ⁺ cation, classified at a DMA voltage of approx. 950 V, in a 0.8 mMolar solution, versus electrospray generator runtime. The applied high voltage potential to the liquid sample was +2.8 kV.	55
5.20	Particle concentration of the TDDABr ⁺ ion, classified at a DMA voltage of approx. 1400 V, in a 0.8 mMolar solution, versus electrospray generator runtime. The applied high voltage potential to the liquid sample was +2.8 kV.	55
5.21	Particle concentration of the TPtAl ⁺ cation, classified at a DMA voltage of approx. 550 V, in a 0.05 mMolar solution, versus electrospray generator runtime. The applied high voltage potential to the liquid sample was +2.3 kV.	56
5.22	Particle concentration of the TPtAl ⁺ ion, classified at a DMA voltage of approx. 1950 V, in a 0.05 mMolar solution, versus electrospray runtime. The applied high voltage potential to the liquid sample was +2.3 kV. At 1213 seconds the main concentration increases as the high voltage potential was decreased to +2.0 kV.	56
5.23	Particle concentration of the THA ⁺ cation, classified at a DMA voltage of approx. 690 V, in a 0.2 mMolar solution, versus electrospray runtime. The applied high voltage to the liquid sample was +2.8 kV.	57
5.24	Particle concentration of the THABr ⁺ ion, classified at a DMA voltage of approximately 1030 V, in a 0.2 mMolar solution, versus electrospray runtime. The applied high voltage to the liquid sample was +2.8 kV. .	57
5.25	NSD of Negative Ion Clusters	58
5.26	NSD of Positive Ion Clusters	59
5.27	Comparison of Different Positive Ion Clusters	60

6.1	Mäkelä Fit for Kilpatrick's Mass-Mobility Relation	63
6.2	Atomic Mass vs. Mobility Equivalent Diameter according to Kilpatrick's Relation	63
6.3	Mass versus Electrical Mobility of Tetraalkyl Ammonium Haldies (TMAI = Tetramethyl ammonium Iodide, TPrAI = Tetrapropyl Ammonium Iodide, TBAI = Tetrabutyl Ammonium Iodide, THABr = Tetraheptyl Ammonium Bromide, TDABr = Tetradecyl Ammonioium Bromide, TDDABr = Tetradodecyl Ammonium Bromide and TPtAI = Tetrapentyl Ammonium Iodide).	64